Chapter 1 INTRODUCTION

1.1 Motivation

An increasing demand for high data rates in wireless communications has made it essential to investigate methods of achieving high spectral efficiency which would take into account the wireless channel. Adaptive modulation is one such scheme proposed by Hanzo and Torrance [1] which helps to maximize the data rates that can be transmitted over wireless channels. The technique accomplishes this by adapting to the changing channel conditions and by making use of spectrally efficient modulation schemes like Quadrature Amplitude Modulation (QAM) [2]. As compared to QAM, adaptive modulation achieves similar spectral efficiency with better energy efficiency. When channel conditions are poor, energy efficient schemes such as BPSK or QPSK are used. As channel quality improves, 16-QAM or 64-QAM are used. Adaptive modulation tends to work more effectively in slow fading channels, since channel quality doesn't change drastically from frame to frame and the frame rate is the rate of adaptation.

Adaptive modulation finds its application in wireless data systems which unlike voice systems, don't necessarily require a constant data rate. This allows the data rate to increase during good channel conditions and overall higher throughputs can be achieved. Recently, adaptive modulation has been proposed for the third generation packet data standard titled *cdma2000 1xEV-DO*[1]. This is also branded as "High Data Rate" or HDR. In order to optimize the throughput and make the best use of the available bandwidth, the proposed HDR system sends and receives at different data rates. The data rate continuously changes as the channel conditions change. Thus, it employs adaptive modulation to achieve high throughput by adapting the modulation based on the channel variations.

[1] The 1x prefix is to represent the fact that the chip rate 1 times the 1.2288 Mega chips per second chip rate of a standard IS-95 CDMA channel. 'EV' stands for "Evolution" since it is an evolution of second generation CDMA. DO represents "Data-only" to emphasize the fact that it is optimized for data and not voice.

1.2 Significance of this thesis

The main objective of this thesis is to provide an investigation of two practical issues impacting adaptive modulation for wireless communications. Adaptive modulation is a promising way to achieve high data rates. It utilizes modulation such that it can provide better spectral efficiency (for a given energy efficiency) by adapting to higher modulation schemes like QAM based upon the channel conditions. QAM is sensitive to channel estimation since it requires an estimation of the amplitude variations in the channel in addition to knowledge of the phase variations. As a result, adaptive modulation is also sensitive to the accuracy of such knowledge. In this thesis we investigate several channel estimation techniques and their impact on the performance on adaptive modulation. This is the first major contribution of this thesis. In order to accurately adapt the modulation scheme, the channel quality must be known at the transmitter. This requires the channel quality to be estimated by the receiver and fed back to the transmitter. The second contribution of this thesis is the investigation of channel quality estimation (specifically SNR estimation) on the performance (including both error performance and spectral efficiency) of adaptive modulation.

1.3 Overview of thesis

This thesis is organized as follows. In Chapter 2, we discuss different channel equalization[2] techniques and evaluate the factors which affect the channel estimators. Chapter 3 presents an overview of adaptive modulation and investigates the impact of feedback delays, Doppler frequency and channel estimation on its performance. In Chapter 4, we investigate SNR estimation. Specifically, we investigate two short-term

[2] Note that we use the term 'equalization' in a manner that is slightly different from traditional usage. Traditionally, 'equalization' refers to frequency domain equalization which is necessary in frequency selective channels. Here, we refer to time domain equalization which is necessary for amplitude modulation in flat (or frequency selective) fading.

SNR estimation techniques and their impact on the performance of adaptive modulation in various channel conditions. Secondly, we investigate long-term SNR estimation and its use in adaptive modulation. The two general techniques are compared in terms of their overall performance and their degradation compared to ideal estimation. The key factors considered are Doppler frequency, feedback delays and the SNR estimation technique. Finally, Chapter 5 concludes the thesis and provides directions for further research.

Chapter 2 EQUALIZATION TECHNIQUES FOR QAM

2.1 Introduction

The objective of this chapter is to discuss equalization techniques for QAM in the presence of the Rayleigh fading. By the term "equalization" we mean the removal of phase and amplitude distortion in the time domain introduced by the wireless channel. This is to be contrasted with the traditional use of term in the case of constant amplitude modulation schemes where "equalization" is used for frequency domain equalization in frequency selective channels.

The rapid growth in the mobile communications has given rise to an increasing demand for channel capacity using limited bandwidth. Quadrature amplitude modulation (QAM) yields the high spectral efficiency owing to its use of amplitude as well as phase modulation and therefore is an effective technique for achieving high channel capacity. Application of QAM for land mobile communication in the presence of a rapidly fading channel is challenging because of the amplitude distortion introduced and thus requires high quality channel estimation and equalization. Many researchers [3], [4], [5], [6] have studied pilot symbol assisted modulation (PSAM) for compensating for the effects of fading at the receiver. We will investigate different equalization techniques and the effect of pilot symbol spacing and Doppler spread on the performance of PSAM using 16-QAM and 64-QAM in this chapter.

2.2 Fundamentals of Pilot Symbol Assisted Modulation

In PSAM, a known pilot symbol and information symbols are multiplexed in the time domain [i.e. time division multiplexing or TDM] at the transmitter [7].

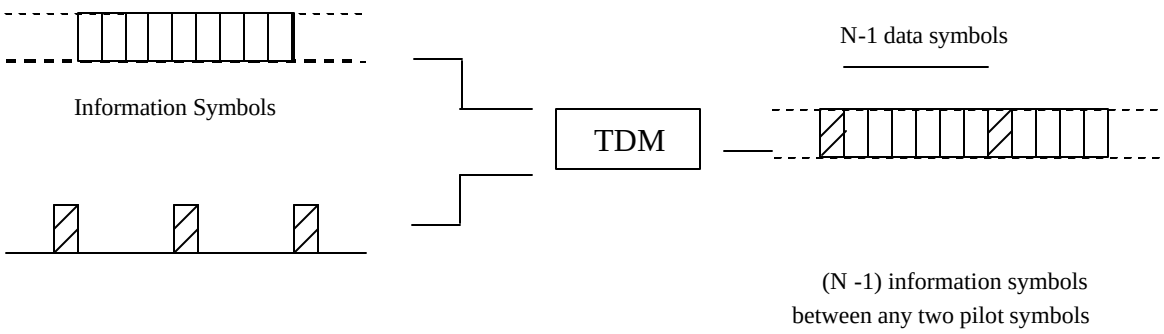

Figure 2.1 Frame format for PSAM

The pilot symbols are inserted periodically into the useful information sequence prior to pulse shaping. Applying the Nyquist sampling theorem, we have a required relationship between the Doppler frequency F_d, symbol period T_s and the frame length N (also pilot symbol spacing since there is one pilot per frame):

$$F_d T_s \leq \frac{1}{2N} \tag{2.1}$$

This equation shows that the pilot symbols should be inserted more frequently as the Doppler rate increases. A frame having N symbols consists of one pilot symbol followed by (N-1) information symbols. Figure 2.1 shows the frame format for PSAM.

Table 2.1 Pilot symbols used in different modulation schemes

Modulation	**Number of bits per symbol**	**Pilot Symbol**
BPSK	*1*	1+j0
QPSK	*2*	1+j
16 QAM	*4*	3+j3
64 QAM	*6*	7+j7

Equation (2.1) tells us how frequently we must sample the channel based on the Nyquist sampling theorem. However, we must remember that at the receiver our samples are inherently noisy. Thus, the energy per pilot symbol is important since it will determine the signal-to-noise ratio (SNR) of the samples. In order to maximize the SNR of the channel samples without introducing excess gain, we choose the symbol with the largest energy in its symbol set as shown in Table 2.1. Figure 2.2 shows the signal constellation for 16-QAM and 64-QAM with dark dots representing possible pilot symbols with signal power 18 and 98 respectively.

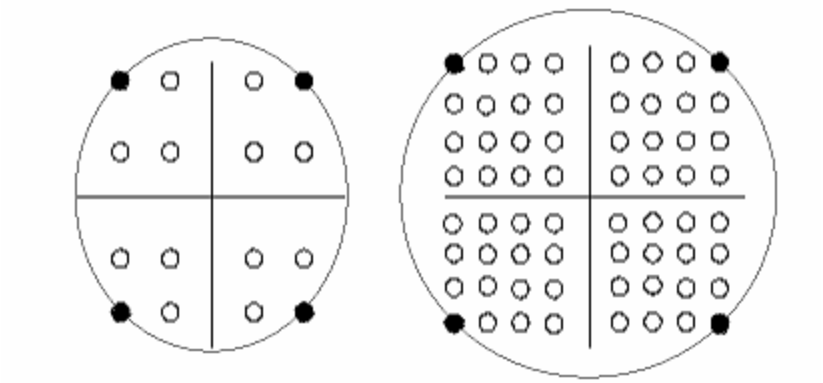

16 QAM 64 QAM

Figure 2.2 Signal constellations of QAM indicating possible pilot symbol

After matched filtering, the receiver demultiplexes the pilot symbols and the information symbols. The extracted sequence of pilot symbols is then processed to remove the modulation and interpolated to give an estimation of the fading distortion for the information symbols. Thus, the amplitude and phase variation due to fading can be estimated for every data symbol. The estimates are used to equalize the information symbols prior to detection.

2.3 Wireless channel model

In mobile wireless communication systems, the channel is time varying because of the motion of either the transmitter or the receiver which results in propagation path changes. If the channel bandwidth is greater than the signal bandwidth, then the received signal will undergo *flat fading*. The main characteristics of flat fading channels are deep fades caused by multipath. If there is no line-of-sight component in the received signal, Rayleigh fading describes the statistical distribution of the received envelope of a flat fading signal.

2.3.1 Rayleigh fading phenomenon

The Rayleigh distribution has a probability density function (pdf) given by (Figures 2.3, 2.4) [8]

$$p(r) = \frac{r}{s^2}\exp\left[\frac{-r^2}{2s^2}\right] \text{.....} (0 \le r \le \infty)$$

$$0\text{…….....} (r < 0) \qquad (2.2)$$

where s is the rms value of the received voltage signal and s^2 is the time average power of the received signal. The probability that the envelope of the received signal does not exceed a specific value R is given by the corresponding cumulative distribution function (CDF)

$$P(R) = Pr(r \le R) = \int_0^R p(r)dr = 1 - \exp\left[\frac{-R^2}{2s^2}\right] \qquad (2.3)$$

The power spectrum of the Rayleigh fading signal with a uniform angle-of-arrival distribution from 0 to 2p describes the time varying nature of the signal and is given by [8]

$$S(f) = \frac{1.5}{p\, f_d \sqrt{1 - \left(\frac{f - f_c}{f_d} \right)^2}} \tag{2.4}$$

where f_d is the maximum Doppler frequency and f_c is the carrier frequency. Figures 2.5 and 2.6 show the power spectral density and the corresponding temporal correlation due to the multipath fading.

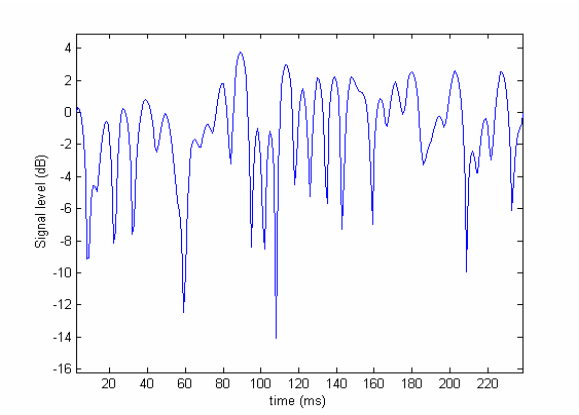

Figure 2.3 A typical Rayleigh fading envelope as a function of time

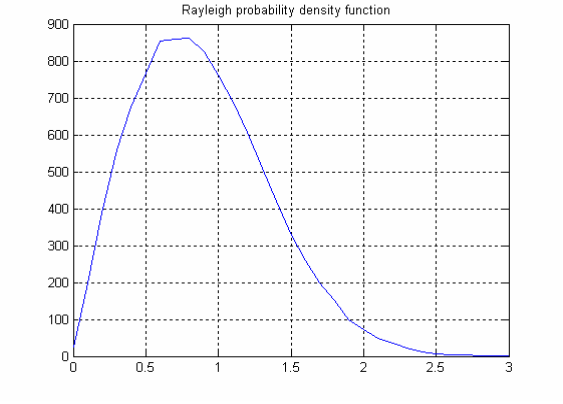

Figure 2.4 Rayleigh probability density function (pdf)

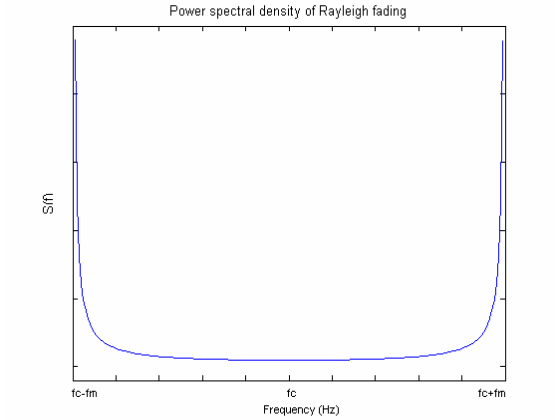

Figure 2.5 Fading power spectrum density

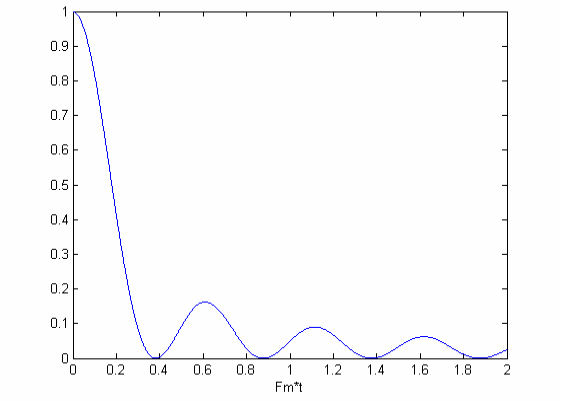

Figure 2.6 Temporal correlation of the fading waveform

2.3.2 Jakes model for Rayleigh fading

The classic Jakes model [9] is among the simplest of all the different types of methods for generating a flat Rayleigh fading channel. This model assumes that the transmitted signal is vertically polarized. Figure 2.7 shows a typical component wave incident on the mobile.

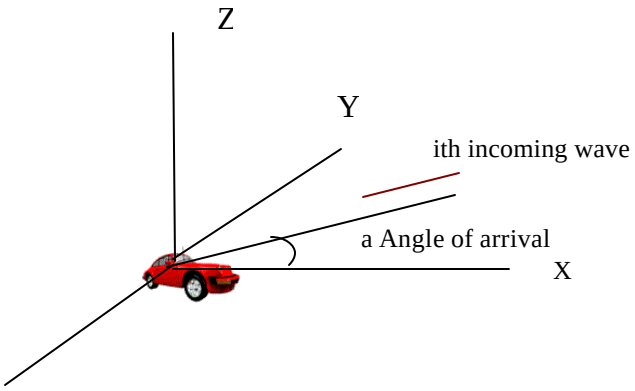

Figure 2.7 Model for a component radio wave incident on the mobile

Mobility introduces a Doppler shift f_i in every wave, which is given by [9]

$$f_i = cos\ a_i * F_d \tag{2.5}$$

where F_d is the maximum Doppler frequency and α_i is the angle-of-arrival for the *i*th wave. The fading signal is then the summation of the field components over all the sinusoids as in equation 2.6 where a_i is the angle of arrival and ? $_c$ is the carrier frequency.

$$E_z = E_o \sum_{i=1}^{N} \cos(w_c t + a_i) \tag{2.6}$$

The autocorrelation function of the channel power gain over time is given as [5]

$$A_g(t) = J_0^2(2\pi v t / \lambda)$$

where v is the mobile user's velocity and λ is the wavelength of the carrier. Figure 2.6 plots the temporal correlation of the channel. Note that maximum Doppler frequency is related to the mobile velocity by

$$F_d = v / \lambda$$

2.4 Transmitter and Receiver Models

Figure 2.8 shows the configuration of the transmitter and receiver. The data is modulated using the desired modulation scheme using Gray coding. After modulation, a known pilot symbol is inserted at the first position in the frame with *(N-1)* information data symbols following. The frame length is *N* symbols. The signal is then transmitted over a channel with flat Rayleigh fading and additive white Gaussian noise (AWGN). After matched filtering, the receiver extracts the pilot symbols, and interpolates them to form an estimate of the channel state for each data symbol time. The complex baseband model of the received signal *r(t)* is given by :

$$r(t) = s(t)c(t) + n(t) \tag{2.7}$$

where *s(t)* : transmitted baseband signal

c(t) : fading distortion

n(t) : additive white Gaussian noise

and all quantities are complex due to the nature of the modulation schemes used.

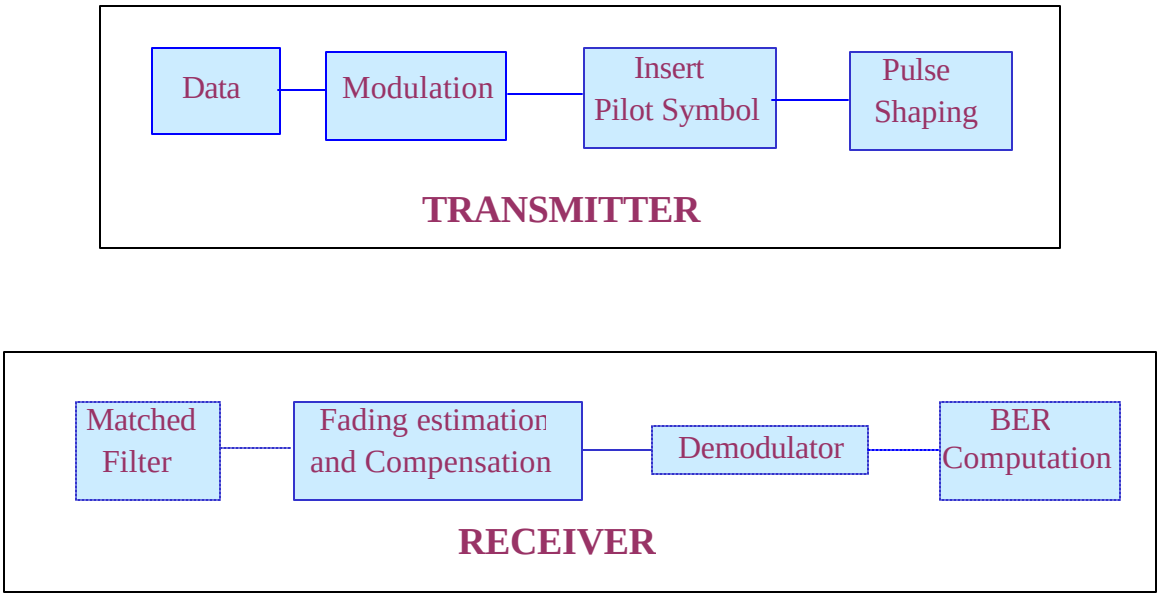

Figure 2.8 Configuration of the transmitter and receiver

If the estimated channel coefficients are represented by $\hat{c}(t)$, then the transmitted signal can be estimated as

$$\hat{s}(t) = f\left\{\frac{r(t)}{\hat{c}(t)}\right\}$$

$$= f\left\{\frac{c(t)}{\hat{c}(t)}s(t) + \frac{n(t)}{\hat{c}(t)}\right\} \qquad (2.9)$$

where f{.}is an appropriate decision function.

2.5 Gaussian Interpolation

Gaussian interpolation is one of the simpler interpolation schemes [6], [7]. The estimated fading variation at $t = (k + m/N)\, T_F$ using Gaussian interpolation is given by

$$\hat{c}((k+m/N)T_F) = \sum_{i=-1}^{1} Q_k(m)\bar{c}((k+i)T_F) \tag{2.10}$$

Where T_F = frame duration

m = 0, 1, 2 ... (N-1)

N = frame length

and the weighting factors for second order Gaussian interpolation are expressed as

$$Q_{-1}\left(\frac{m}{N}\right) = \frac{1}{2}\left\{\left(\frac{m}{N}\right)^2 - \left(\frac{m}{N}\right)\right\} \tag{2.10a}$$

$$Q_0\left(\frac{m}{N}\right) = 1 - \left(\frac{m}{n}\right)^2 \tag{2.10b}$$

$$Q_1\left(\frac{m}{N}\right) = \frac{1}{2}\left\{\left(\frac{m}{N}\right)^2 + \left(\frac{m}{N}\right)\right\} \tag{2.10c}$$

In the case of zeroth-order interpolation, the weighting factors are given by

$$Q_{-1}\left(\frac{m}{N}\right) = 0 \tag{2.11a}$$

$$Q_0\left(\frac{m}{N}\right) = 1 \tag{2.11b}$$

$$Q_1\left(\frac{m}{N}\right) = 0 \tag{2.11c}$$

For first order interpolation, weighting factors are given by

$$Q_{-1}\left(\frac{m}{N}\right)=0 \tag{2.12a}$$

$$Q_0\left(\frac{m}{N}\right)=1-\left(\frac{m}{N}\right) \tag{2.12b}$$

$$Q_1\left(\frac{m}{N}\right)=\frac{(m-1)}{N} \tag{2.12c}$$

The fading distortion is estimated by using equation (2.9) at the fading distortion compensator as shown in Figure 2.9.

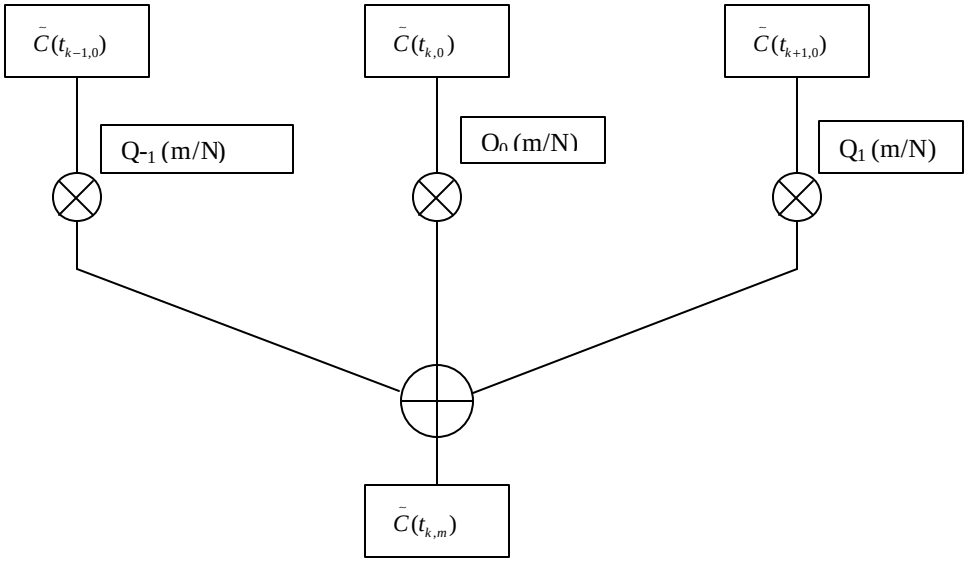

Figure 2.9 Fading distortion compensator

2.6 Wiener Interpolation

Let *r(iN)* be the *K*-length column vector, $-\lfloor K/2 \rfloor \le i \le \lfloor K/2 \rfloor$ which is formed from the received pilot symbols divided by the known pilot symbols. This gives us the estimated distortion in the pilot symbols at the receiver. To estimate the distortion coefficients for the data symbols, we calculate the coefficient vector *h(k)* which satisfies the **Wiener-Hopf** equation [3].

$$\boldsymbol{Rh(k) = w(k)} \tag{2.13}$$

where *w(k)* and *R* are the estimated autocorrelation of the received signal and the correlation between the received signal and the data and are calculated using equations (2.14) and (2.16):

$$w_i(k) = \gamma n(N-1)\left(\frac{q}{q+1}\right)\tilde{R}_c((i-k)NT) + \delta_{ik} \tag{2.14}$$

where q is the ratio of the pilot power to the data power, g is the ratio of the energy per bit to the noise power and

$$\delta_{ik} = \begin{bmatrix} 1 & 0 & 0 \\ 0 & 1 & 0 \\ 0 & 0 & 1 \end{bmatrix} \tag{2.15}$$

The autocorrelation of the received signal is

$$R_{ik} = \gamma n \frac{(N-1)}{\tilde{b}} \left(\frac{q}{q+1}\right) \tilde{R}_c((i-k)\,NT) \tag{2.16}$$

where $\tilde{R}_c(\tau)$ is the normalized version of the autocorrelation function of the channel's complex gain given by:

$$\tilde{R}_c(\tau) = \exp(j2p\,F_D\tau)\,J_0(2p\,F_D\tau) \tag{2.17}$$

where the maximum Doppler frequency is given by F_d. The coefficient vector h is calculated to satisfy the Wiener–Hopf equation. As can be observed, the Wiener filter requires prior information of the Doppler frequency and signal-to-noise ratio to estimate of the fading channel.

2.7 FFT Interpolation

An important application of the FFT algorithm is in FIR linear filtering of long data sequences. The FFT algorithm takes *N* points of input data and transforms the *N* points into the frequency domain by taking the fast version of the Discrete Fourier Transform (DFT) of the input data [5], [10]. The input data to the FFT channel estimator is the ratio of the received pilot symbols to the known pilot symbols. This factor gives a measure of the distortion that the pilot symbol has undergone due to the flat fading. Figure 2.10 shows the general FFT algorithm. Both *N* and N_p should be power of 2 in order to use FFT and IFFT. Note, that DFT can be used if a power of two is not possible, but the efficiency of the transform is sacrificed. *G(n*) is the output of the DFT. Provided equation (2.1) is satisfied *G(n)* has all the components of the fading channel, and near $n = N_p$, *G' (n= 0)*. Therefore we can interpolate from $2N_p$ symbols to $2NN_p$ symbols with zero insertion. Interpolation is carried out as follows:

$$G'(n) = NG(n).....[0 \le n \le (\tfrac{N_P}{2} - 1)] \qquad (2.18)$$

$$G'(n) = 0.....\left[\frac{N_P}{2} \le n \le \left(\frac{N_P}{2} - 1\right)\right]$$

$$G'(n) = NG[n - N_P(N-1)].....\left[\frac{N_P}{2}(2N-1) \le n \le N_P N - 1\right]$$

Where G' (n) is considered to be periodic, that is

$$G'(m+2NN_pr) = G'(m) \qquad (r = 0, \pm 1, \pm 2 \ldots) \qquad (2.19)$$

This zero insertion in the frequency domain is equal to interpolation between the pilot symbols in the time domain. This scheme is simple because only the FFT and zero insertion are required [5].

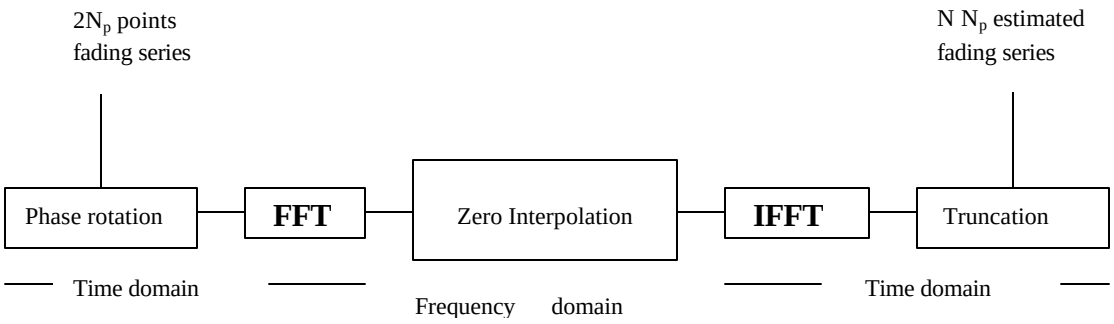

Figure 2.10 General FFT algorithm

The inverse FFT (equation (2.20)) of the sampled frequency data is performed in the last stage to get the time-domain data.

$$c(k) = \frac{1}{NN_P} \sum_{n=0}^{NN_P} G'(n) \exp\left(j \frac{2p\,nk}{NN_P} \right) \ldots\ldots\ldots (k = 0,1,\ldots\ldots, NN_p - 1) \qquad (2.20)$$

2.7.1 Edge effects due to FFT interpolation

The FFT interpolation method estimates the channel distortion from the pilot symbols very efficiently but generates leakage due to the truncation required to obtain a finite length sampled data. When truncation is done the frequency data as calculated by taking the FFT of the distortion pilot samples is not truly equal to zero beyond the frequency range of the channel. Forcing these values to zero causes edge effects in the final channel estimate as shown in Figure 2.12. To avoid this edge effect, it is necessary that the time interval width of g is an integer multiple of $1/f_d$. However, it is difficult (if not impossible) to select the sampling frequency and the truncation time to satisfy this requirement. We therefore solve this problem by introducing extra frames in the beginning and in the end of the target frames (as shown in Figure 2.11) and then applying FFT interpolation. After obtaining the samples in the time domain, we consider only our target frames and discard extra frames that we introduced for channel estimation. This helps reduce the edge effect, although it does introduce additional delay. Figure 2.12 illustrates the effect of the leakage on the BER curve for 16-QAM and 64-QAM. As can

be observed there is an improvement of 5dB at an SNR of 25dB for 16-QAM and 64-QAM when accounting for the edge effect.

Figure 2.11 Frame structure to reduce edging effect

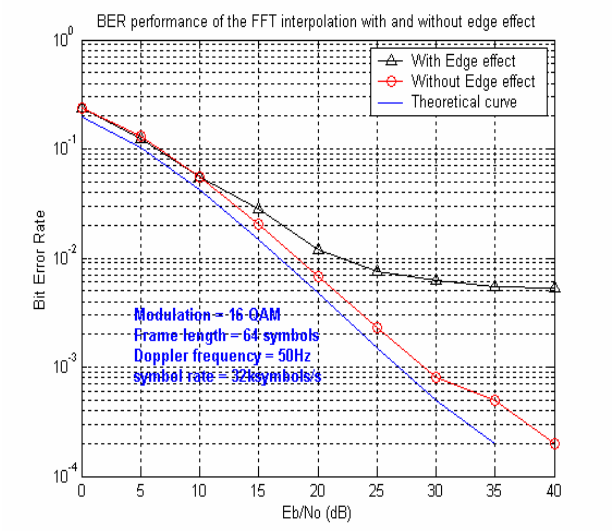

Figure 2.12 (a) BER performance with and without the edge effect for 16-QAM and Doppler frequency = 50Hz

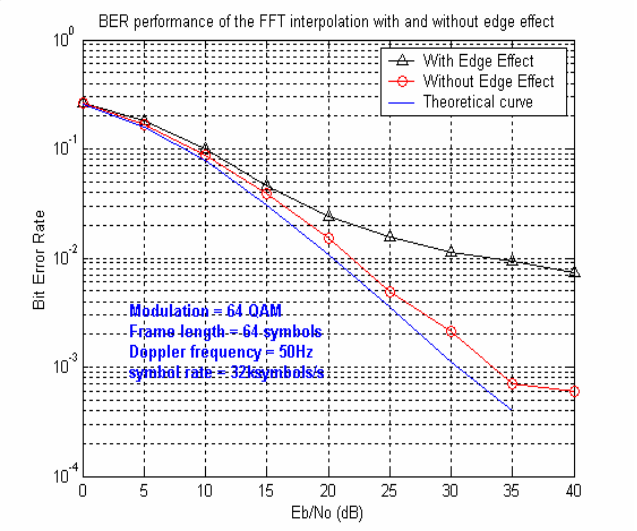

Figure 2.12 (b) BER performance with and without the edge effect for 64-QAM and Doppler frequency = 50Hz

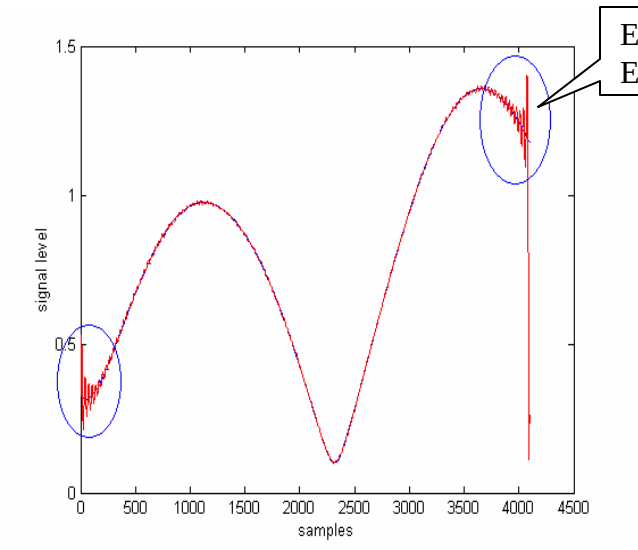

Figure 2.12 (c) Illustration of the edge effects in the channel envelope

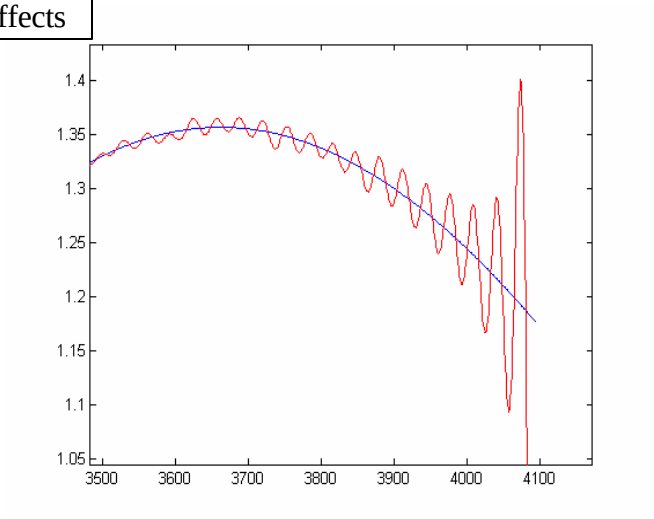

Figure 2.12 (d) Shows enlarged portion of the edge effects in the channel envelope of Figure 2.9 (c)

2.8 Simulation Results

2.8.1 Effect of interpolation order on the Gaussian Interpolator

We first examined the performance of QAM with Gaussian interpolation. It was found that (not surprisingly) the BER performance of QAM improves as the interpolation order increases. Table 2.2 summarizes the various parameters used in the simulations for the zeroth, first and second order Gaussian interpolator.

Table 2.2 Specifications for Gaussian interpolation

Frame length	32 symbols
No. of frames	32
No. of pilots in each frame	1
Doppler frequency	20 Hz
Symbol rate	10 ksymbols/s
Frame duration	3.2 ms
Second order (m = 31; N = 32)	
Q_{-1}	0.5 *(((m-1)/N)^2 - (m-1)/N)
Q_0	1-((m-1)/N)^2
Q_1	0.5 *(((m-1)/N)^2 + (m-1)/N)
First order (m = 31; N = 32)	
Q_{-1}	0
Q_0	1-(m-1)/N
Q_1	(m-1)/N
Zeroth order	
Q_{-1}	0
Q_0	1
Q_1	0

As can be seen from Figure 2.13 (a-b-c), the estimated fading envelope traced by the different interpolation orders of the Gaussian interpolator improves considerably as the order is increased from 0 to 1. Second and first order interpolation does a significantly better job than the zeroth order. There is little difference between first and second order interpolation. First order interpolation doesn't trace the true fading envelope as accurately as second order especially near deep fades where second order does better. Figure 2.13 shows that as the interpolation order increases, the BER performance improves for

Gaussian interpolation as expected. Further, there is a substantial improvement in performance in going from zeroth to first order interpolation, but little advantage in going to second order interpolation. Thus, the BER results bear out the observations from the estimation plots.

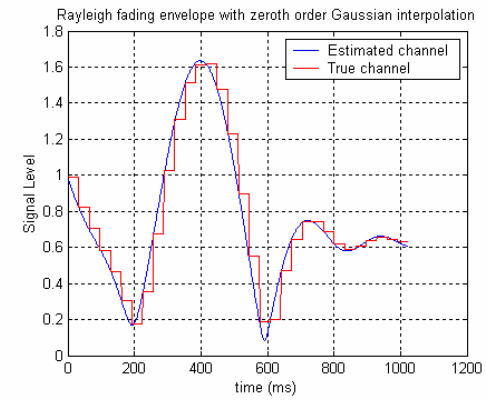

Figure 2.13(a) The estimated fading envelope as traced by the zeroth order interpolation

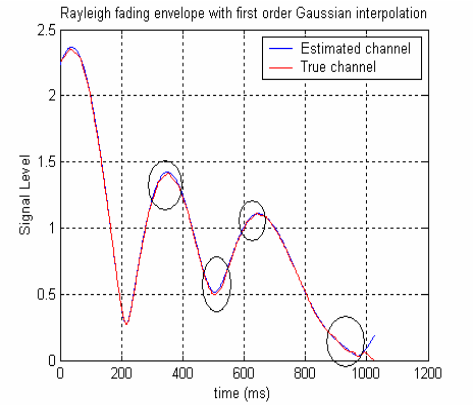

Figure 2.13(b) The estimated fading envelope as traced by the first order interpolation

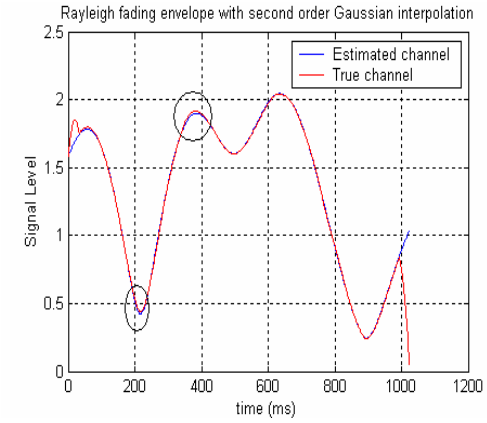

Figure 2.13 (c) The estimated fading envelope as traced by the second order interpolation

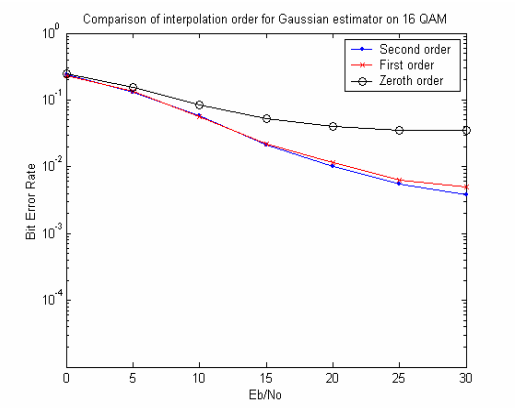

Figure 2.13 BER performance of 16-QAM using different interpolation orders for Gaussian interpolator at Doppler 50Hz and BER target of 0.1%

2.8.2 Effect of the Doppler spread

Doppler spread is defined as the range of frequencies over which the channel Doppler spectrum is non-zero. The amount of spectral broadening depends on F_d which is a function of the velocity of the mobile and the wavelength of the carrier. As shown in Figure 2.7, when the *i*th path arrives at an angle of a with respect to the motion of the mobile unit, its frequency is shifted by

$$F_i = F_d \cos(?) \tag{2.21}$$

$$F_d = v/? \tag{2.22}$$

where *?* is carrier wavelength and v is the velocity of the mobile.

Figure 2.14 presents simulation results which highlight the impact of different Doppler spreads on the BER of 16-QAM when using Wiener and FFT channel estimators. Figure 2.15 presents results for all three interpolation schemes. It can be seen that BER performance degrades as the Doppler frequency increases [3], [11]. However, the FFT interpolation technique is nearly unaffected by Doppler frequency until F_d exceeds 400Hz. This is in stark contrast to the other two interpolation techniques which degrade consistently as Doppler increases. Note that at rates above 500Hz, the sampling frequency of the channel does not meet the Nyquist rate.

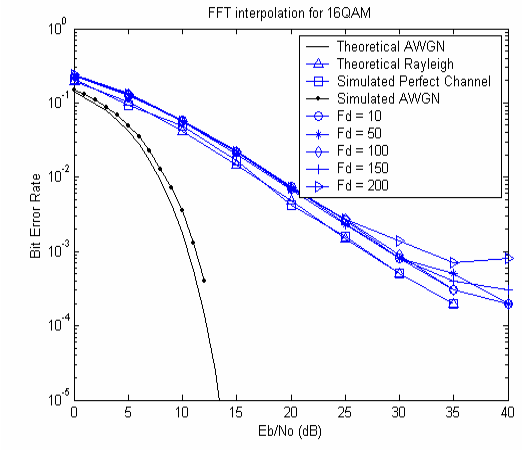

Figure 2.14 (a) Impact of Doppler spread on FFT interpolation for 16-QAM

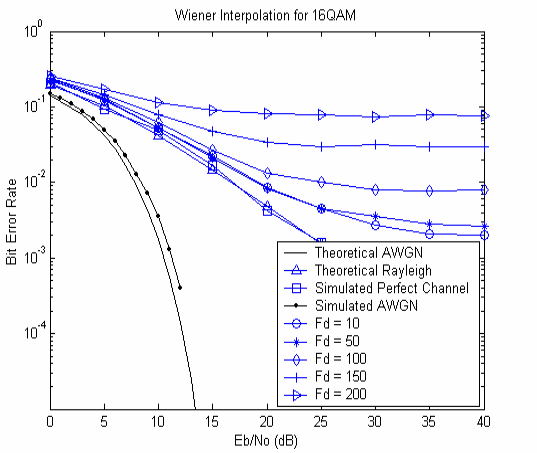

Figure 2.14 (b) Impact of Doppler spread on Wiener interpolation for 16-QAM

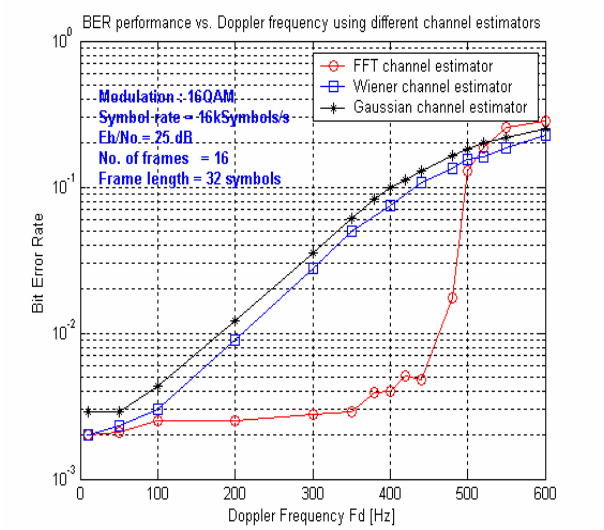

Figure 2.15 Effect of Doppler frequency on 16-QAM performance

2.8.3 Effect of pilot symbol spacing

Insertion of pilot symbols results in wasting energy, so there is a tradeoff between wasting energy in unnecessary pilot symbols and not sampling the fading process often enough for good estimation. When the Doppler frequency is more than the theoretical limit, the channel estimator is not able to compensate for the distortion. This can be verified from equation (2.1). For example (using equation (2.1)): If the frame length N = 64 symbols and F_s = 16 kHz then any channel estimator works as long as

$$F_d < 125\ Hz$$

Figure 2.16 (a, b) show how the true fading envelope is traced by FFT interpolation at Doppler rates of 120 Hz and 130 Hz for the same pilot symbol spacing. As can be seen, for Doppler spread = 130 Hz, the envelope is not accurately traced unlike at 120 Hz. This can also be observed from the signal constellations which demonstrate how well the received data symbols are compensated when compared to the transmitted data symbols. From Figure 2.16(d-e), we have verified that when the Doppler (F_d) = 125Hz the channel estimator is unable to provide accurate compensation for the Rayleigh fading distortion.

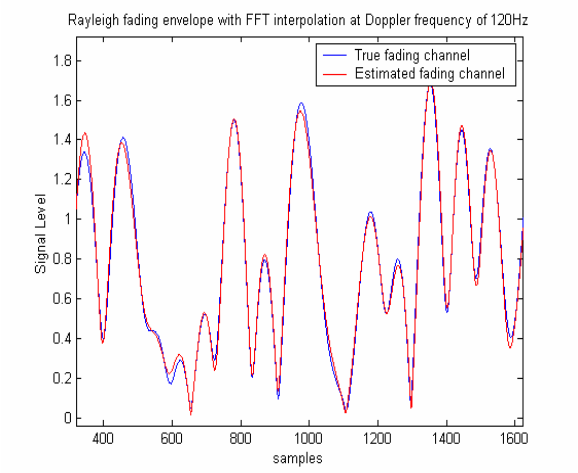

Figure 2.16 (a) Fading envelope for Doppler frequency of 120 Hz

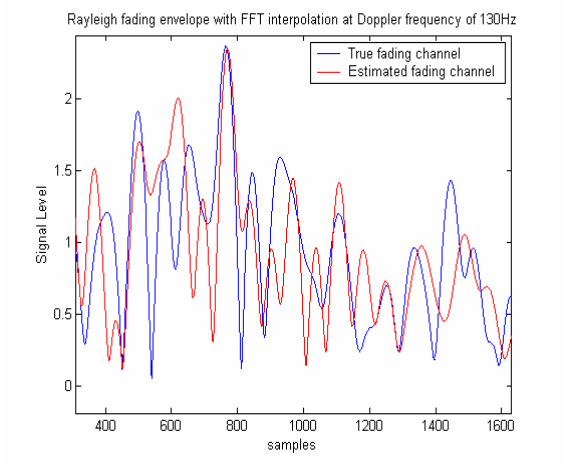

Figure 2.16 (b) Fading envelope for Doppler frequency of 130 Hz

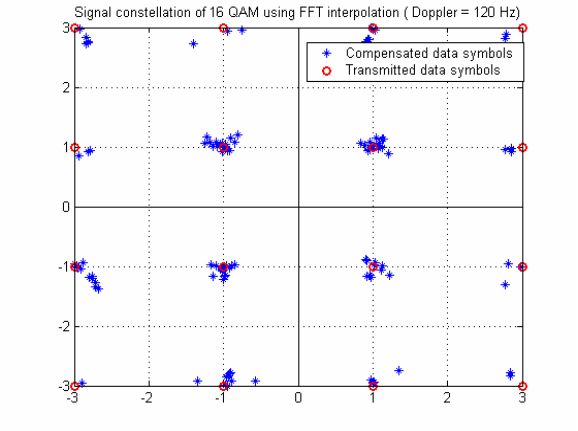

Figure 2.16 (c) Signal constellation for 16-QAM at Doppler frequency of 120 Hz

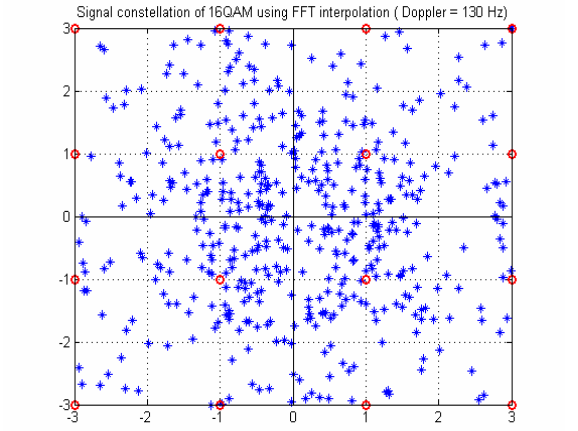

Figure 2.16 (d) Signal constellation for 16-QAM at Doppler frequency of 130 Hz

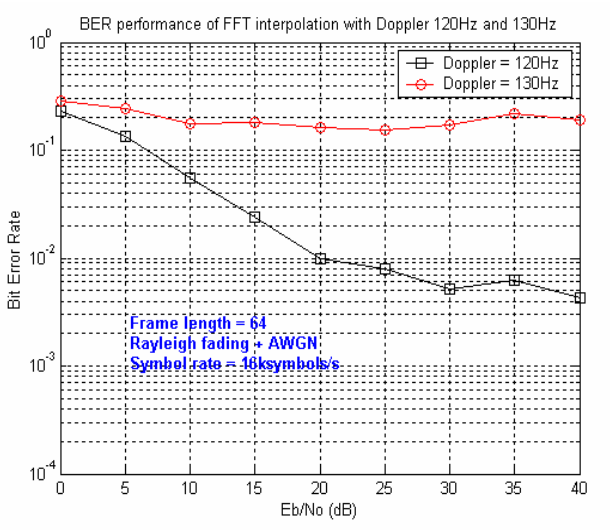

Figure 2.16 (e) BER performance of 16-QAM with Doppler of 120 Hz and 130 Hz

This can also be seen by varying the pilot symbol spacing for a constant Doppler rate. Figure 2.17 shows the effect of pilot symbol spacing using different channel estimators on the performance of 16-QAM. As can be observed, for the case of F_dT=0.04 and E_b/N_o=30dB, beyond a pilot symbol spacing of 16, the channel estimators are ineffective. Also, since $F_dT = 0.04$, equation (2.1) is violated when $N > 12$.

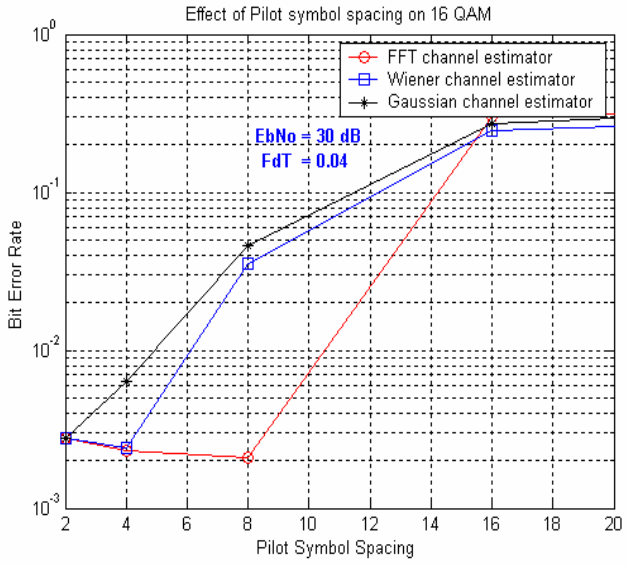

Figure 2.17 BER vs. Pilot symbol spacing for 16QAM

It should be noted that the power loss due to the insertion of the pilot symbols is given by

$$Pl = 10\log\left(\frac{N}{N-1}\right)(dB) \tag{2.23}$$

Therefore, if a frame has 32 symbols, then it would result in 0.13 dB power loss due the pilot symbol.

2.8.4. Effect of the Pilot SNR

As mentioned in section 2.2, we choose the pilot symbol with the highest amplitude among the signal constellation. Since the data samples received at the receiver are very noisy, it is essential to have high pilot SNR. This is done by increasing the pilot amplitude so that it gets less distorted and helps in more accurate estimation of the distortion coefficients for the data. Thus, the higher the pilot amplitude, the higher the pilot SNR and thus the more accurate the estimation of the distortion at the receiver using these pilot samples will be.

2.8.5. Comparison of channel estimators

The FFT interpolator performs better than Wiener and Gaussian interpolators at moderate to high Dopplers. As the Doppler frequency (Figure 2.15) or the pilot symbol spacing (Figure 2.17) increase, the FFT estimator is able to compensate for the distortion more effectively than the other two estimators. Also, as the fading becomes more rapid, more accurate channel estimation is required. The FFT estimator translates the received pilot symbols in the frequency domain, inserts zero and then reconverts into the time domain. This method results in more accurate estimation in both slow and fast fading as discussed in section 2.7.2. Figure 2.18 shows how the received data symbols are compensated as compared to the transmitted data symbol using Wiener and FFT interpolation assuming

the parameters presented in Table 2.3. It is observed that when using Wiener interpolation, the compensation is inferior as compared to the compensation achieved using the FFT interpolator. Also, the Wiener estimator requires prior information regarding the Doppler frequency and signal-to-noise ratio to estimate the fading channel. Finally, the Gaussian estimator results in an error floor and is inferior to the other techniques.

Table 2.3 Specifications used for the simulation results of Figures 2.18

Modulation	64 QAM
Pilot symbol spacing	16
Doppler frequency	50Hz
Frame length	16 symbols
Symbol rate	10kHz
Legends for Figures 2.18	red asterix: transmitted symbols black dot : compensated data symbols

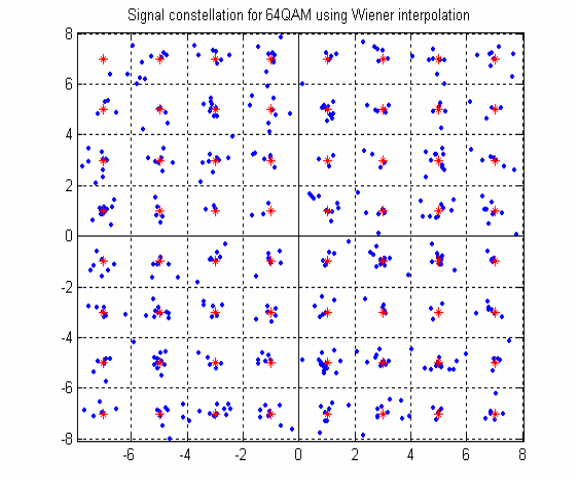

Figure 2.18 (a) Signal constellation of 64 QAM using Wiener interpolation

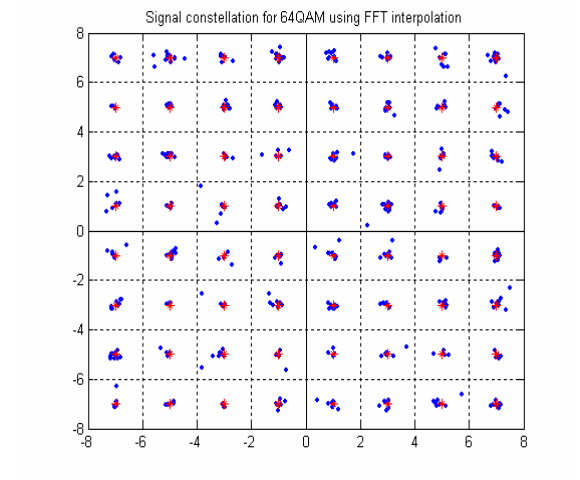

Figure 2.18 (b) Signal constellation of 64 QAM using FFT interpolation

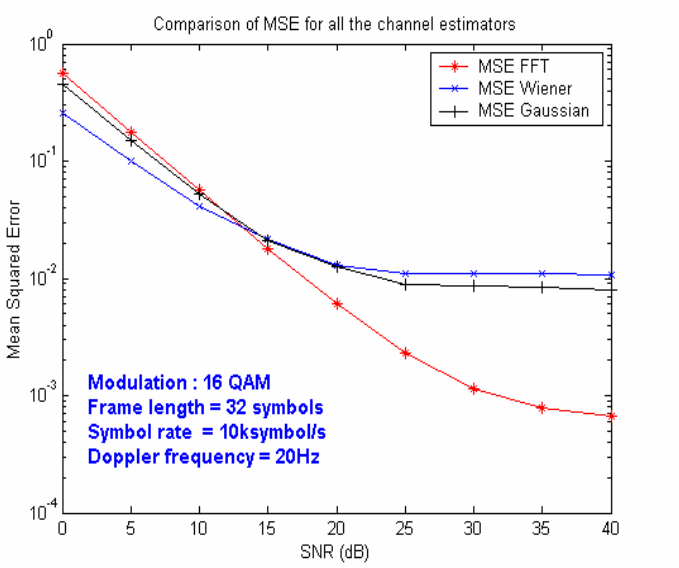

Figure 2.19 Comparison of Mean squared error

Figure 2.19 shows a comparison of the mean square error for all the channel estimators.

Table 2.4 Specifications used for the simulation results of Figures 2.19

Modulation	16 QAM
Pilot symbol spacing	16
Doppler frequency	20Hz
Frame length	32 symbols
Symbol rate	10kHz
Frame rate	312Hz

It is observed that at lower SNRs, the Wiener estimator performs the best and as the SNR increases, the performance of the FFT interpolator becomes the superior technique. Also, after an SNR of 20 dB, the Gaussian and Wiener interpolators result in an error floor whereas the FFT technique doesn't suffer an error floor until approximately 35dB. Figure 2.20 shows the spectrum for the estimated and true fading channels using all channel

three estimators. It can be observed that the spectrum of the estimated channel using the FFT estimator is a closer approximation of the true channel spectrum as compared to the Gaussian and Wiener estimators.

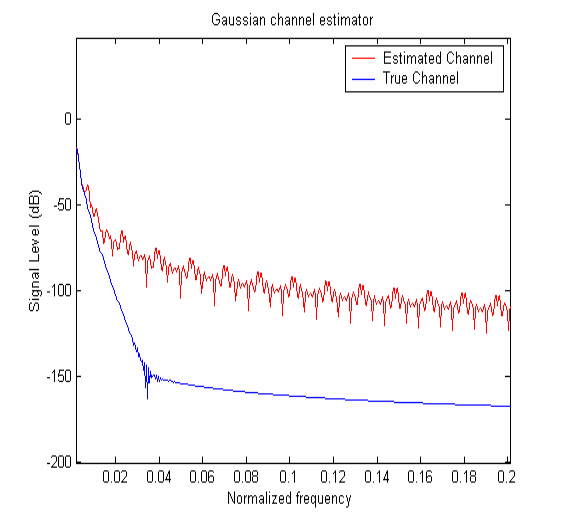

Figure 2.20(a) Spectral plot of the channel using Gaussian interpolation

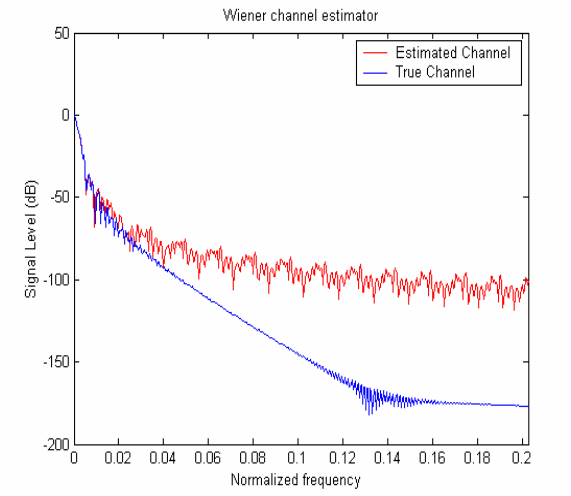

Figure 2.20(b) Spectral plot of the channel using Wiener interpolation

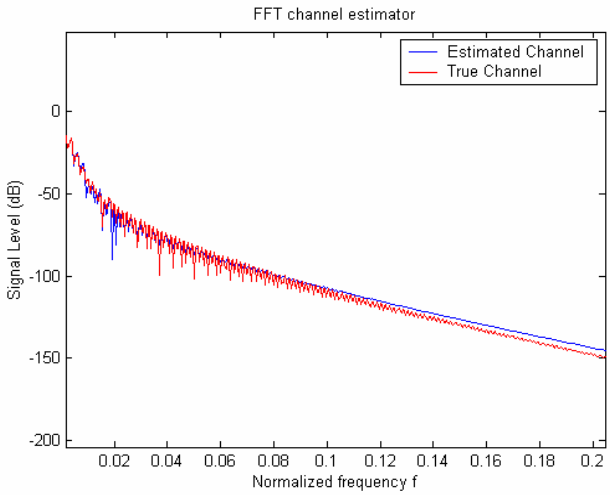

Figure 2.20(c) Spectral plot of the channel using FFT interpolation

2.8.6 Analysis of the Effect of Channel estimation error on *M*-QAM BER Performance in Rayleigh fading

PSAM based channel estimation has been studied by several authors [3,4,8]. In all these studies, the only analytical result for comparison is a tight upper bound on the BER for *M*-QAM, which doesn't consider different parameters of the various channel estimators. Here we calculate the theoretical BER of 16-QAM with general PSAM based channel estimation. Goldsmith discusses channel estimation error with only amplitude error and then with amplitude as well as phase errors in [12]. We shall also study these effects in the following sections using FFT interpolation. Table 2.5 summarizes the parameters that are used in the equations discussed in the following sections.

Table 2.5 summarizes the parameters that are used in the Equation 2.24

a , ?	Amplitude and phase of the true channel
$\hat{a}$,$\hat{q}$	Amplitude and phase of the estimated channel
O	$E\{\alpha^2\}$
$\hat{\Omega}$	$E\{\hat{\alpha}^2\}$
r	$\hat{\Omega}/\Omega$
?	Correlation coefficient between a and $\hat{a}$
$\bar{g}$	O *g

2.8.6.1 Amplitude estimation error only

In this section, we compare our PSAM based simulation results with the theoretical BER of *M*-QAM with PSAM in flat Rayleigh fading channels. Initially, we assume that we know the phase information of the fading channel at the receiver (via a digital Costas loop or other method) and we estimate the amplitude of the channel coefficients using FFT interpolation. Table 2.6 lists all the coefficients in the BER calculation (equation 2.26) of 16-QAM.

Table 2.6 Coefficients in the BER of 16QAM

i	**? i**	**a_i**	**b_i**
	¼ *	$\sqrt{1/5}$ *	$\sqrt{1/5}$ *
1	1	3	0
2	1	1	0
3	1	3	-2
4	-1	3	2
5	1	-1	2
6	1	1	2

The theoretical BER of 16-QAM for a PSAM based channel estimator as calculated in [12] is given by:

$$BER_{16\,qam}(g) = \sum_{i=1}^{6} w_i \mathrm{I}(a_i, b_i, \bar{g}, r, r) \tag{2.24}$$

where

$$I(a_i, b_i, \bar{g}, r, r) = \frac{(1-r)}{p} \int_0^{p/2} \int_{-p/2} (\sin 2q\, J_2(\sqrt{r}\sin 2q \sin\Phi + 1, \sqrt{(1-r)\bar{g}}\,(a\cos q + \sqrt{r} b \sin q)))/(\sqrt{r}\sin 2q \sin\Phi + 1)^2$$

$$\text{and} \quad J_2(a,b) = \frac{1}{2} - \frac{3b}{4\sqrt{2a+b^2}} + \frac{b^3}{4(2a+b^2)^{3/2}} \tag{2.25}$$

We calculate *r* and ρ as defined in Table 2.5. Table 2.7 gives the values of *r* and ρ for 16-QAM.

Table 2.7 gives the values of r and ρ for 16-QAM

E_b/N_o (dB)	**r**	r
0	1.0134	0.8468
10	1.0317	0.9880
20	1.0003	0.9981
30	1.0002	0.9999
40	1.0015	0.9999

As seen from the Table 2.7, *r* is very close to 1 so we have approximated *r* to be 1 in our analysis whereas ρ increases towards 1 as the average SNR per bit increases. This is expected because, as defined in Table 2.5, ρ is the correlation coefficient between the true and the estimated channel which becomes better with the average SNR per bit. Figure 2.21 shows the simulated and theoretical curves with only amplitude error. We can see that the simulated curve follows theoretical curve very closely. As compared to perfect channel estimation, there is a degradation of 1dB with amplitude error only.

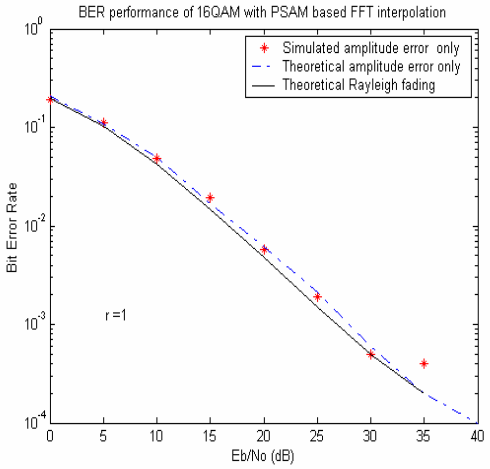

Figure 2.21 Simulated and Analytical Performance of 16-QAM with only amplitude error

2.8.6.2 Amplitude and phase estimation error

In this section, we estimate the theoretical BER for PSAM with no prior knowledge of amplitude or phase available at the receiver. Equation (2.26) defines the pdf of the phase estimate error [12] where phase estimation error is defined by ψ.

$$y = q - \hat{q}$$

$$p(y) = \frac{(1-r)}{4p^2}\left[\frac{\sqrt{1-q^2} + q(p - \cos^{-1} q)}{\sqrt{1-q^2}^3}\right](2p - |y|) \tag{2.26}$$

where $q = \sqrt{r}\cos y$.

The BER of 16-QAM is given by

$$p_{16QAM}(g) = \sum_{i=1}^{12} w_i I(a_{1i}, a_{2i}, b_i, \bar{g}, r, r) \tag{2.27}$$

where

$$I(a_{1i}, a_{2i}, b_i, \bar{g}, r, r) = \frac{(1-r)}{p}\int_{-2p}^{-2p}\int_{0}^{p/2}\int_{-p/2}^{p/2}\frac{\left(\sin 2q\, p(y).J_2(\sqrt{r}\sin 2q + 1, \sqrt{(1-r)\bar{g}}.((a_1\cos y + a_2\sin y)\cos q + \sqrt{r}b\sin q))\right)}{(\sqrt{r}\sin 2q\sin j + 1)^2} dj\, dq\, dy \tag{2.28}$$

and the coefficients *w,a1,a2,b* are listed in Table 2.8.

Table 2.8 Coefficients in the BER Calculation of 16-QAM with amplitude and phase error

i	w_i	a_{1i}	a_{2i}	b_i
	1/8 *	$1/\sqrt{5}$ *	$1/\sqrt{5}$ *	$1/\sqrt{5}$ *
1	1	3	1	0
2	1	3	3	0
3	1	1	1	0
4	1	1	3	0
5	1	3	1	-2
6	1	3	3	-2
7	-1	3	1	2
8	-1	3	3	2
9	1	-1	1	2
10	1	-1	3	2
11	1	1	1	2
12	1	1	3	2

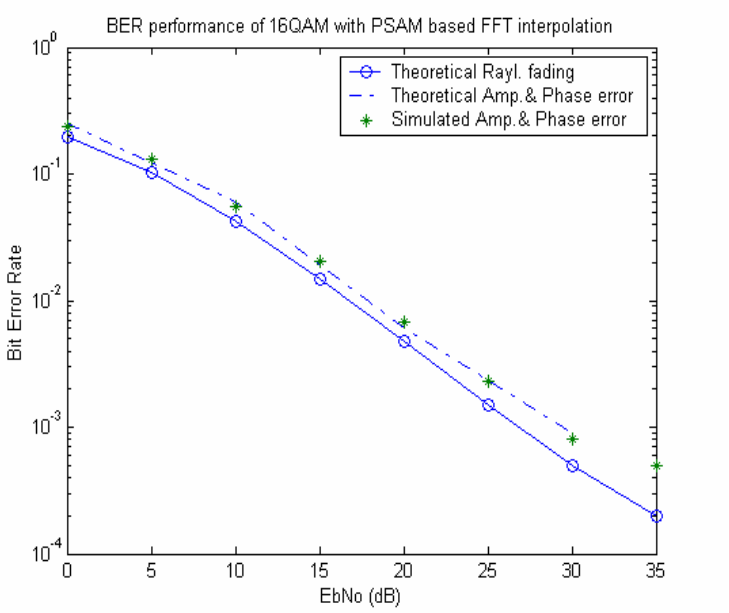

Figure 2.22 Simulated and Analytical Performance of 16-QAM with amplitude and phase error

Figure 2.22 shows the simulated and theoretical curves for 16-QAM with amplitude and phase error. Again, we find that the simulated results follow the theoretical curve very closely. As compared to the case of perfect estimation, there is a degradation of 2 dB in performance with amplitude and phase error.

2.9 Chapter summary

In this chapter we have discussed PSAM-based channel estimators. Using pilot symbols, the receiver obtains amplitude and phase estimates by interpolating the channel coefficients. Simulation results using different channel estimators along with the effect of pilot symbol spacing and Doppler frequency were discussed. We found that PSAM is relatively simple to implement and effectively compensates channel distortion for QAM modulation schemes. We also compared our simulation results with theoretical amplitude and phase estimation error results for the BER of 16-QAM. Specifically, the analytical results were compared to simulated results with FFT interpolation. In Chapter 3 we will discuss the impact that these estimators have on the performance of adaptive modulation.

Chapter 3 INTRODUCTION TO ADAPTIVE MODULATION

3.1 Introduction

Wireless channels vary over time due to fading and changing interference conditions. Adaptive modulation exploits these variations to maximize the data rate that can be transmitted over such channels in an energy efficient manner. This requires use of spectrally efficient modulation schemes such as Quadrature Amplitude Modulation (QAM). Multilevel QAM makes it possible to achieve high spectral efficiency while employing PSAM based channel estimators, which were discussed in Chapter 2. The objective of this chapter is to study modulation-level-controlled adaptive modulation proposed by Torrance and Hanzo [1] and to extend their work to examine the effect of channel estimation and equalization, feedback delay, and Doppler spread. In this chapter, we will initially assume perfect knowledge of the channel to examine the effect of delay and Doppler spread on adaptive modulation, and then examine the impact of channel estimation and equalization. In the next chapter we will examine the impact of channel quality estimation.

3.2 Motivation

The main aim of adaptive modulation is to achieve high capacity (i.e., high spectral efficiency) in a power efficient manner. One immediate question would be whether or not we should adapt power and modulation (i.e., rate). To answer this question, we shall discuss adaptive modulation from on information theory perspective. Specifically we will examine the Shannon capacity of the fading channel with power and rate adaptation strategies [13].

Variable power and rate:

If *S(?)* is the transmit power relative to an instantaneous channel SNR of ?, the Shannon capacity of a fading channel with bandwidth = *B* and average power S_{AV} is given by :

$$C = \max_{s(g):\int S(g)p(g)dg = \bar{S}} \int_0^\infty B\log_2(1+\frac{S(g)g}{S_{AV}})p(g)dg \tag{3.1}$$

$$S_{AV} \geq \int_0^\infty S(g)p(g)dg \tag{3.2}$$

where *p(g)* is the SNR distribution. The power adaptation strategy that optimizes (3.1) can be shown to be:

$$\frac{S(g)}{S_{AV}} = \begin{cases} \frac{1}{g_0} - \frac{1}{g}, g \geq g_0; \\ 0, g < g_0 \end{cases} \tag{3.3}$$

where $?_0$ is the cut-off threshold for allocating power and is determined as in [9]. If ? is less than the threshold value then no power is allocated. We can summarize the expression of equation (3.3) as follows. When the power is good, we allocate power, but when the channel is bad we do not. The final expression for the channel capacity is obtained by substituting the 3.3 into 3.1. The resulting spectral efficiency is given by:

$$\frac{C}{B} = \int_{g_0}^\infty \log_2(\frac{g}{g_0})p(g)dg \tag{3.4}$$

Constant power:

In the case of constant transmit power, the transmitted power is same as the average power therefore the spectral efficiency is:

$$\frac{C}{B} = \int_0^{\infty} \log_2(1+g)p(g)dg \tag{3.5}$$

We observe from equations (3.4) and (3.5) (and their plots in Figure 3.1) that there is a very small difference in the spectral efficiency (C/B) between optimal power and rate allocation and rate adaptation with constant power.

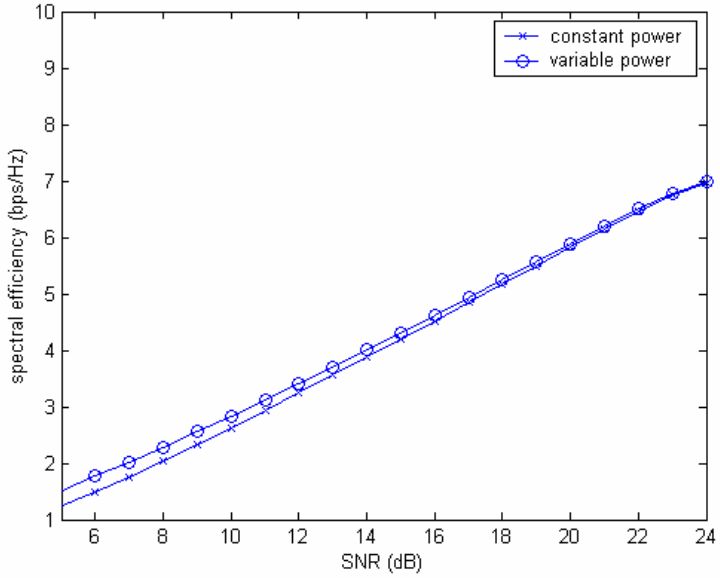

Figure 3.1 Spectral efficiency of constant and variable power

This motivates us to examine rate (or modulation) adaptation schemes rather than power control schemes. This is in contrast to traditional cellular systems that attempt to use power control with constant data rate. In this chapter we shall assume constant power strategy while examining adaptive modulation.

3.3 Adaptive Modulation

The main concept of adaptive modulation is to maintain a constant performance by varying transmitted power level, modulation scheme, coding rate or any combination of these schemes [13]. This allows us to vary the data rate without sacrificing BER performance. Since in land mobile communication systems, the local mean value of the received signal level varies due to the fading channel, adaptive modulation is an effective way to achieve high data rates. Here we study the modulation level controlled adaptive modulation proposed by Hanzo and Torrance [1]. We focus our discussion on two significant performance metrics: BER and Spectral efficiency. Spectral efficiency can be defined as the expected value of $\log_2 M$ (number of bits per symbol), where M is the modulation level. The modulation schemes chosen for adaptation in this work are BPSK, QPSK, 16-QAM and 64-QAM offering 1,2,4 and 6 bits per symbol respectively. Also, we consider adaptation on a frame-by-frame basis.

We will examine a threshold based adaptation scheme that switches between the different modulation schemes depending upon the estimated channel SNR during each frame. The channel SNR is estimated at the receiver and is reported to the transmitter through a feedback channel. Rate selection can be done at either the transmitter or receiver. If rate selection is done at the transmitter, more feedback information is required since the SNR must be quantized and transmitted. This information is used to select a modulation scheme for the next transmission frame thereby maintaining the BER below a desired performance threshold. To have a constant estimated channel SNR for all the symbols in the frame we require a slow and flat fading channel [14]. This condition is necessary to insure that channel conditions do not change drastically in the course of a frame. In such a case, the modulation scheme based upon the estimated channel SNR would no longer be optimal for the active frame. We will examine the impact of violating this assumption later in this chapter and in the next chapter. In this chapter we will examine the impact of fading rate on the performance of adaptive modulation directly, whereas in Chapter 4 we will examine the impact of fading rate on channel quality (i.e., SNR) estimation. Figure 3.2 gives an overview of the adaptive modulation.

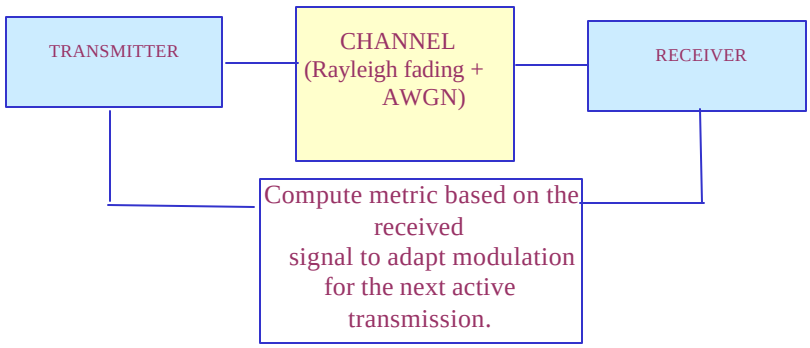

Figure 3.2 Basic flow diagram of adaptive modulation

As mentioned earlier, modulation is adapted on the basis of the channel SNR estimated from the received signal. Three sets of switching levels for the modulation schemes were assumed and correspond to the SNR at which QPSK, 16-QAM and 64-QAM achieve 0.1%, 1% and 10% BER in a Gaussian channel. The reason that we use AWGN performance to choose the thresholds is that during the frame we assume constant SNR, i.e., AWGN conditions. The SNR ranges corresponding to the three different BER targets are described in Table 3.1. Figure 3.3 shows these BER levels with the theoretical curves for different modulation schemes in AWGN.

Table 3.1 Summary of Switching Levels

Conditions on estimated SNR	Modulation adapted
BER = 10%	
SNR<= 2dB	BPSK
2dB<SNR<=8dB	QPSK
8dB<SNR<=12dB	16QAM
12dB<SNR<=40dB	64QAM
BER = 1%	
SNR<= 8dB	BPSK
8dB<SNR<=14dB	QPSK
14dB<SNR<=20dB	16QAM
20dB<SNR<=40dB	64QAM
BER = 0.1%	
SNR<= 11dB	BPSK
11dB<SNR<=17dB	QPSK
17dB<SNR<=25dB	16QAM
25dB<SNR<=40dB	64QAM

The performance of adaptive modulation can then be calculated as

$$p_{BER}(\gamma) = M_{BPS}^{-1}\left[1.\int_{0}^{l_2} P_{bpsk}(\gamma).f_\Gamma(g)dg + 2.\int_{l_2}^{l_3} P_{qpsk}(\gamma).f_\Gamma(g)dg + 4.\int_{l_3}^{l_4} P_{16qam}(\gamma).f_\Gamma(g)dg + 6.\int_{l_4}^{\infty} P_{64qam}(\gamma).f_\Gamma(g)dg\right] \quad (3.6)$$

where $f_\Gamma(g)$ is the distribution function of the instantaneous SNR which is assumed to be a Chi-Square distribution with two degrees of freedom (*i.e.*, Rayleigh fading), M_{BPS} refers to the mean number of the bits per symbol, *i.e.*,

$$M_{BPS} = \left[1.\int_{0}^{l_2} f_\Gamma(g)dg + 2.\int_{l_2}^{l_3} f_\Gamma(g)dg + 4.\int_{l_3}^{l_4} f_\Gamma(g)dg + 6.\int_{l_4}^{\infty} f_\Gamma(g)dg\right],$$

l_1, l_2, l_3, l_4 are the levels fixed for QPSK, 16-QAM and 64-QAM, and $P_{bpsk}(\gamma)$, $P_{qpsk}(\gamma)$, $P_{16qam}(\gamma)$, $P_{64qam}(\gamma)$ are the probabilities of bit error of the respective modulation schemes in an AWGN channel with SNR γ. These are given by equations (3.7), (3.8), (3.9) and (3.10):

$$p_{bpsk} = Q\left(\sqrt{2g}\right) \tag{3.7}$$

$$p_{qpsk} = Q\left(\sqrt{g}\right) \tag{3.8}$$

$$p_{16qam} = \frac{1}{4}\left[Q\left(\sqrt{\frac{g}{5}}\right) + Q\left(3\sqrt{\frac{g}{5}}\right)\right] + \frac{1}{2}Q\left(\sqrt{\frac{g}{5}}\right) \tag{3.9}$$

$$p_{64qam} = \begin{cases} \frac{1}{12}\left[Q\left(\sqrt{\frac{g}{21}}\right) + Q\left(3\sqrt{\frac{g}{21}}\right) + Q\left(5\sqrt{\frac{g}{21}}\right) + Q(7\sqrt{\frac{g}{21}}) + Q\left(5\sqrt{\frac{g}{21}}\right) + Q\left(7\sqrt{\frac{g}{21}}\right) + Q\left(11\sqrt{\frac{g}{21}}\right) - Q\left(13\sqrt{\frac{g}{21}}\right)\right] \\ + \frac{1}{6}\left[Q\left(\sqrt{\frac{g}{21}}\right) + Q\left(3\sqrt{\frac{g}{21}}\right) - Q\left(7\sqrt{\frac{g}{21}}\right) + Q\left(9\sqrt{\frac{g}{21}}\right)\right] \\ + \frac{1}{3}\left[Q\left(\sqrt{\frac{g}{21}}\right)\right] + \frac{1}{4}\left[Q\left(3\sqrt{\frac{g}{21}}\right) - Q\left(5\sqrt{\frac{g}{21}}\right)\right] \end{cases} \tag{3.10}$$

Figures 3.4, 3.5, and 3.6 plot the theoretical BER performance of adaptive modulation for three different target error rates in the presence of Rayleigh fading as a function of average SNR. Additionally, each figure includes the performance of the individual modulation schemes for reference. The spectral efficiency for each target error rate is plotted in Figure 3.7.

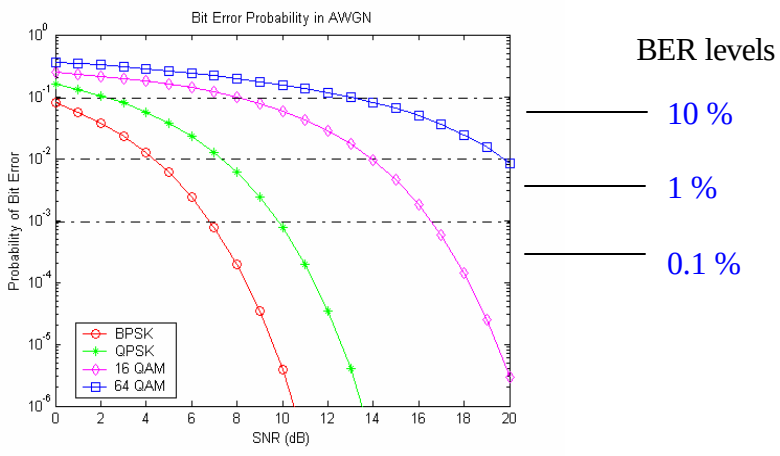

Figure 3.3 Theoretical BER performance in AWGN

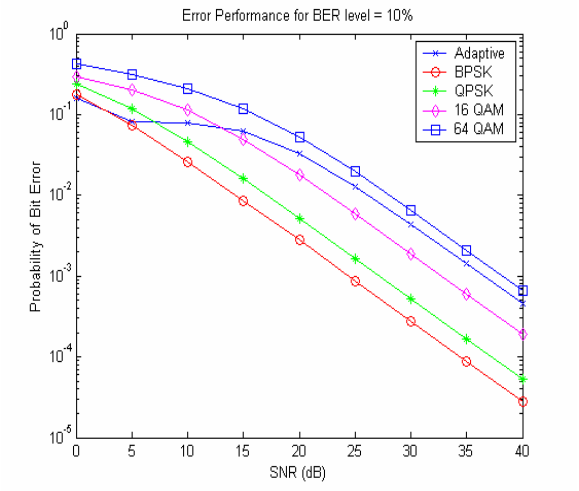

Figure 3.4 Theoretical BER performance of adaptive modulation for BER target of 10 %

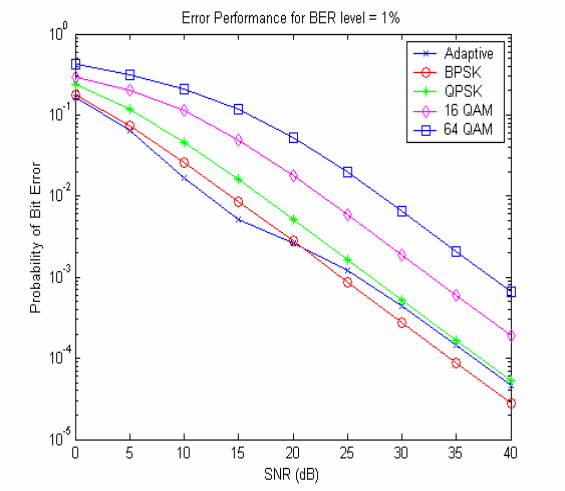

Figure 3.5 Theoretical BER performance of adaptive modulation for BER target of 1 %

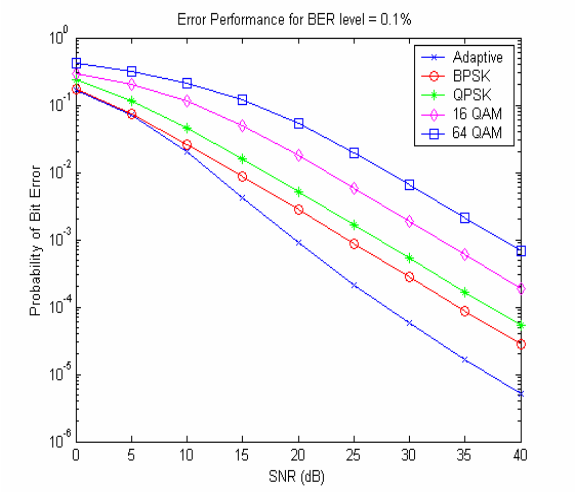

Figure 3.6 Theoretical BER performance of adaptive modulation for BER target of 0.1%

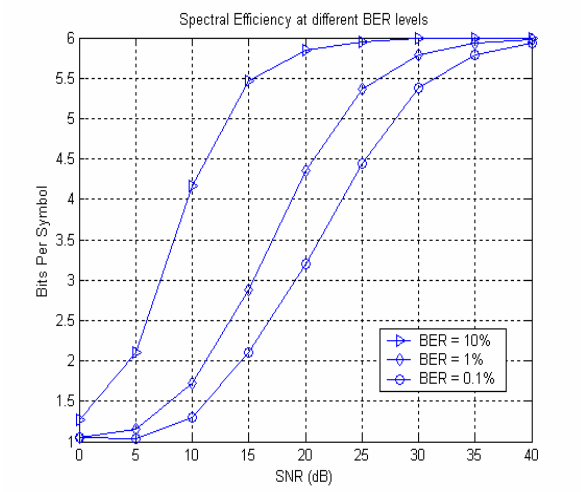

Figure 3.7 Theoretical spectral efficiency of adaptive modulation for all the three BER targets

The first thing to note about the BER performance and spectral efficiency of adaptive modulation, is that no non-adaptive scheme shown provides better performance while simultaneously providing better spectral efficiency. In other words, adaptive modulation provides the best combination of energy and spectral efficiency of any of the modulation schemes. This is to be expected. While fixed schemes either achieve good spectral efficiency or good energy efficiency but not both, adaptive modulation increases spectral efficiency without sacrificing performance. We should also note that choosing a BER target does not guarantee that we will achieve that performance. This is due to the fact that there are a fixed number of modulation schemes. As can be seen in Figure 3.3, at any target error rate there are significant gaps between the chosen modulation schemes. For example, at a target error rate of 1% QPSK requires 8dB of SNR. When the channel SNR is at that value, adaptive modulation will achieve 1% BER. However, for all values between 8dB and 14dB, adaptive modulation will use QPSK and achieve better than 1% BER. Only when the channel reaches 14dB and the modulation scheme switches to 16-QAM will the BER return to the target. Thus, the performance will tend to be better than target as shown in the figures except when the SNR is below the value needed for BPSK to achieve the target.

The other thing to note is the impact of the target BER on spectral efficiency. As we increase the target BER, we increase the spectral efficiency. Thus, we can easily trade performance for spectral efficiency by changing the BER target and thus the switching levels.

3.4 Simulation results

In this section we provide simulation results for adaptive modulation. We initially assume ideal conditions including no feedback delay or error, perfect channel estimation, and perfect channel quality estimation. We will then relax the first two restrictions to examine their impact. In the next chapter we will examine the impact of channel quality estimation.

3.4.1 Ideal Performance

In our initial simulation work we assumed ideal conditions. Specifically, we simulated the performance of adaptive modulation in a Rayleigh fading channel for different BER targets (10%, 1% 0.1%) as described in section 3.3. Figures 3.8, 3.9, and 3.10 show the simulated and theoretical BER performance of the adaptive modulation under ideal conditions.

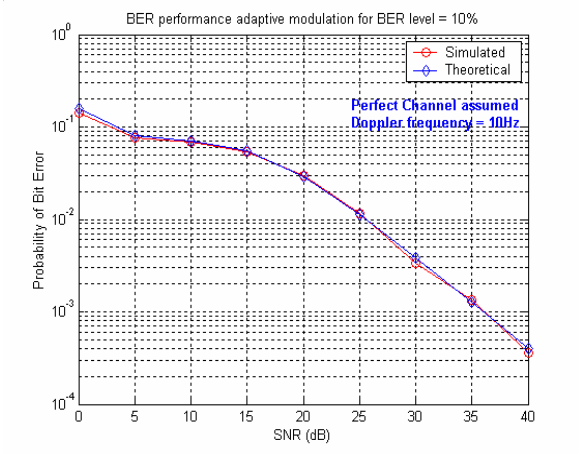

Figure 3.8(a) BER performance of adaptive modulation with perfect channel at **BER = 10%**

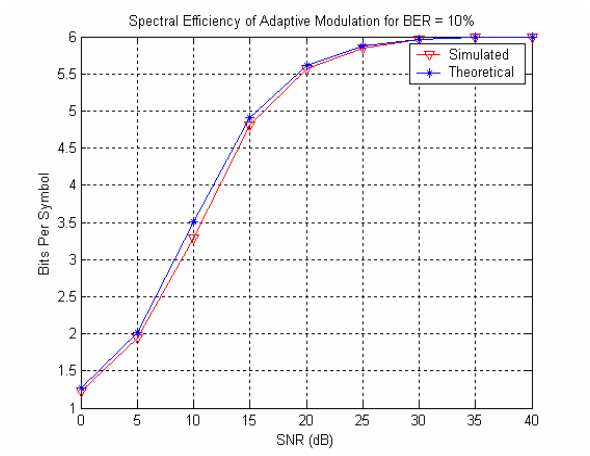

Figure 3.8(b) Spectral Efficiency of adaptive modulation with perfect channel at **BER=10%**

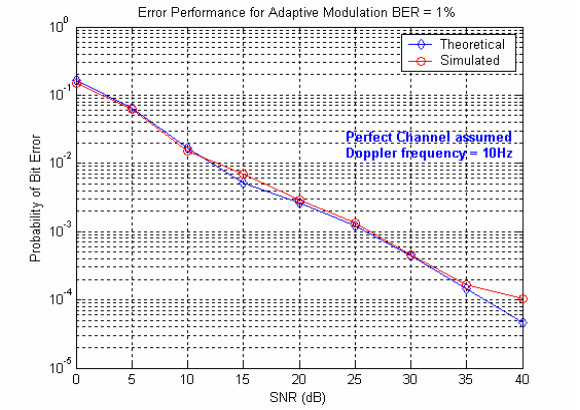

Figure 3.9(a) BER performance of adaptive modulation with perfect channel at **BER = 1%**

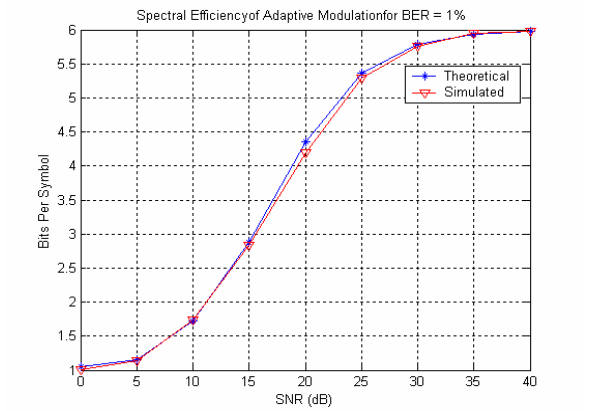

Figure 3.9b) Spectral Efficiency of adaptive modulation with perfect channel at **BER=1%**

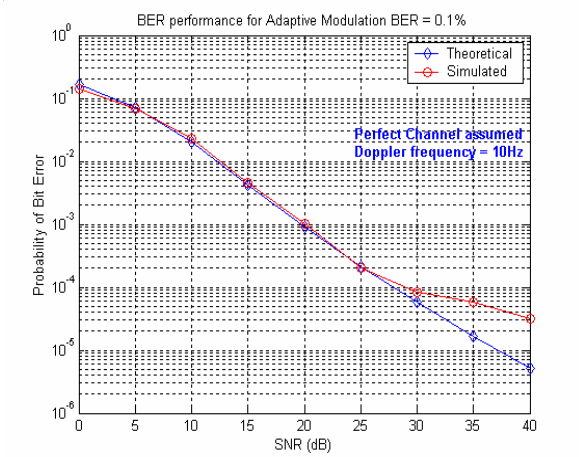

Figure 3.10(a) BER performance of adaptive modulation with perfect channel at **BER= 0.1%**

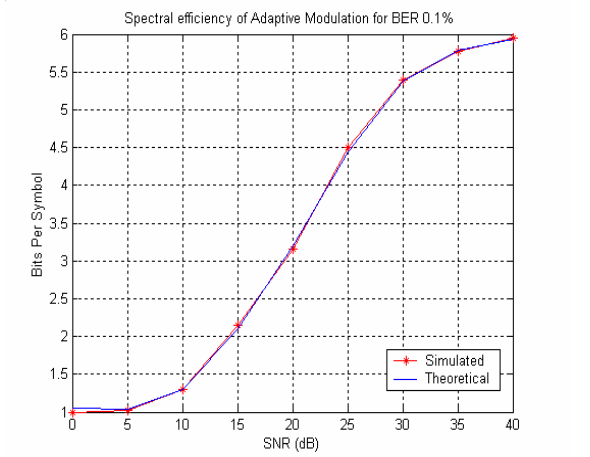

Figure 3.10(b) Spectral Efficiency of adaptive modulation with perfect channel at **BER=0.1%**

Table 3.2 Specifications used for the simulation results of Figures 3.8-3.10

Pilot symbol spacing	64
Doppler frequency	10Hz
Frame length	64 symbols
Symbol rate	32kHz
Frame duration	2ms

We observe that as the SNR increases, spectral efficiency increases, without sacrificing BER performance. Clearly, the target BER cannot be achieved when the SNR is too low (*i.e.,* lower the required SNR for BPSK). However, above that threshold, we achieve the target error rate and increase the spectral efficiency. We also observe that the simulated performance matches the theoretical performance very well, with slight deviation at very low BER values. This deviation is likely due to an inadequacy in the statistical sampling of the error process at extremely low error rates. It's worth noting that at high SNRs the spectral efficiency doesn't achieve 6 bits per symbol for a target BER of 0.1% and 1% whereas for the 10% BER it achieves 6 bits per symbol from 26dB onwards. For higher target BER values, the transmitter selects 64QAM at lower SNRs since it can tolerate a 10% error rate. However, for the other two targets, the modulation schemes fluctuates from 64-QAM to 16-QAM, QPSK and BPSK even at high SNR, keeping the spectral efficiency less than 6 at high SNR values. This can be understood by examining Table 3.2. Table 3.3 provides an overview of frequency of occurrence for each modulation scheme at an average SNR value of 30dB for different BER targets. As can be seen, a higher target error rate corresponds to a higher utilization of 64-QAM and thus a higher spectral efficiency.

Table 3.3 Frequency of Occurrence for different modulation schemes at 30dB average SNR

BER Target	BPSK (%)	QPSK (%)	16QAM (%)	64QAM (%)	Bits Per Symbol
0.1%	4.54	3.57	21.18	70.69	5.2062
1%	1.76	3.92	6.32	88.01	5.6075
10%	3.45	0.54	1.04	94.95	5.7846

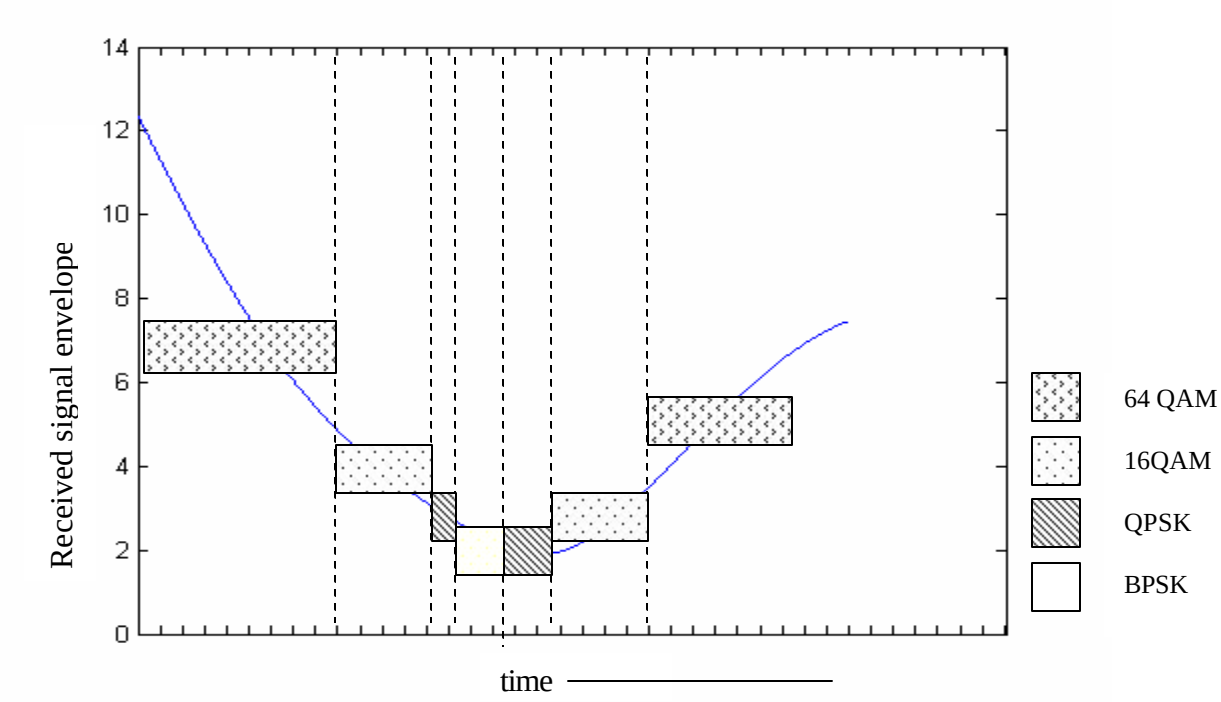

Figure 3.11 A segment of the variations in the fading channel at BER = 1% and 30dB

As an illustration, we show in Figure 3.11 how different modulation schemes are adapted when the Rayleigh fading channel undergoes a deep fade. The figure shows the temporal fluctuation of the received signal envelope along with the corresponding modulation schemes used. As expected the system tends to adapt to BPSK and QPSK in deep fade areas whereas for the good portion of the channel, the modulation is adapted to 64-QAM or 16-QAM. This means that when the channel is not in deep fade the spectral efficiency increases significantly thus providing higher overall data rate.

3.4.2 Effect of feedback delay

As discussed earlier, in adaptive modulation SNR estimates are provided through a feedback channel. Clearly, in a practical system there is some delay between when the channel SNR is estimated and when the new modulation scheme is used. We define this delay in terms of frames and examine the impact of one, two and three frame delays on the performance of adaptive modulation. Figures 3.12 and 3.13 show the simulated results for adaptive modulation with different values of feedback delay but perfect channel estimation and perfect channel quality estimation.

BER = 1%; Doppler frequency = 100Hz

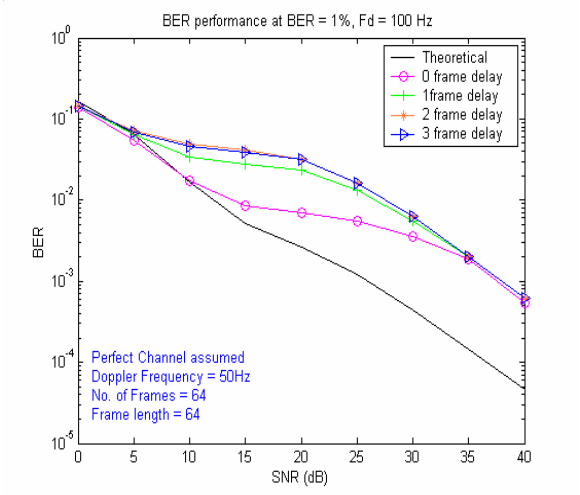

Figure 3.11 (a) BER performance of adaptive modulation in the presence of frame delays

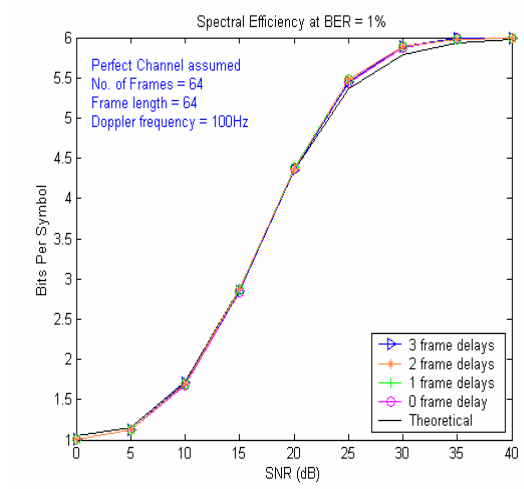

Figure 3.11 (b) Spectral efficiency of adaptive modulation in the presence of frame delays

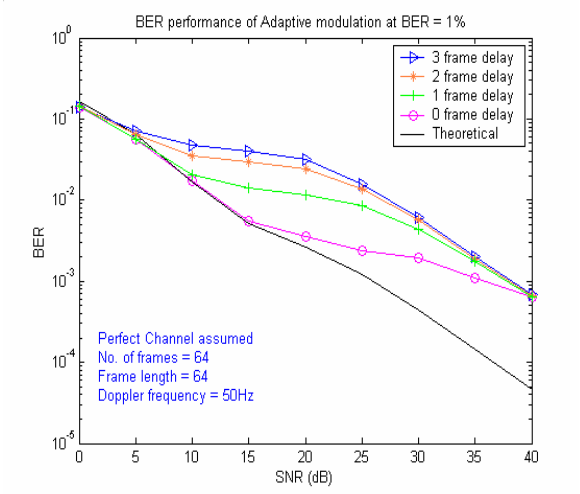

Figure 3.12 (a) BER performance of adaptive modulation in the presence of frame delays

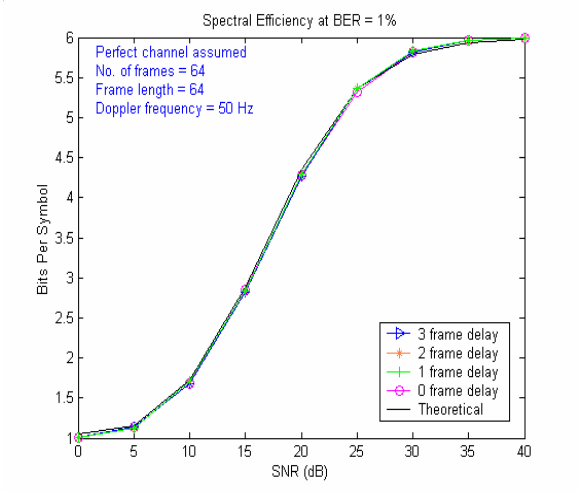

Figure 3.12 (b) Spectral efficiency of adaptive modulation in the presence of frame delays

As expected with an increase in the frame delay, the bit error rate degrades. This is because when there is delay in the system, the channel (and thus the SNR) will change prior to the implementation of the "optimal" modulation scheme. This degrades the BER performance. Note that the degradation with delay is highly dependent on the fading rate. At high Doppler rates the performance will be more sensitive to delay than at low Doppler rates. This can be clearly seen by comparing Figure 3.11(a) which assumes 100Hz and Figure 3.11(b) which assumes 50Hz. We also see that there is degradation even at 0 delay for both Doppler rates. This is in contrast to the simulated performance in Figures 3.8-3.10 which assumed 1Hz Doppler rate. Even with zero delay, high Doppler rates will degrade the performance of adaptive modulation since the channel will change during a frame. Of course the relevant measure here is the ratio of Doppler rate to frame rate. If the Doppler rate is commensurate with the frame rate, performance will degrade from theory. If it is significantly lower than the Doppler rate, it performance will be unaffected.

In Figures 3.11(a) and 3.12(a) we also observe that at higher SNRs, the BER curves for different frame delays converge. This is expected since the modulation scheme adapted at higher SNR's is nearly always 64-QAM and thus the delay impact only affects rare,

deep fades. In the spectral efficiency curves, we observe that there is no change due to the different frame delays. This is because the same modulation schemes are chosen regardless of when they are applied, since the distribution of SNRs does not change. The delay in applying the new modulation scheme only impacts the error rate since the modulation scheme used is no longer appropriate for the channel conditions. We have shown results for different Doppler's 50Hz and 100Hz at BER target of 1% in Figures 3.11 and 3.12.

3.4.3 Effect of Doppler frequency

As discussed in the previous section, we also investigated the effect of the maximum Doppler frequency on the performance of adaptive modulation. Doppler frequency is directly proportional to the mobile velocity, thus as mobile velocity increases, the maximum Doppler frequency increases and faster variations are introduced in the channel causing the performance of adaptive modulation to drop. Figures 3.13 and 3.14 show results for a BER target of 10% and 1% and Table 3.4 summarizes the simulation specifications.

Table 3.4 Specifications used for the simulation results of Figures 3.13-3.14

Pilot symbol spacing	64
Frame length	64 symbols
Symbol rate	32kHz
Frame duration	2ms
Channel conditions	Perfect channel and perfect channel SNR knowledge assumed

It is observed that the bit error rate decreases with the increase in the Doppler frequency even for zero frame delay as discussed previously.

BER = 10%

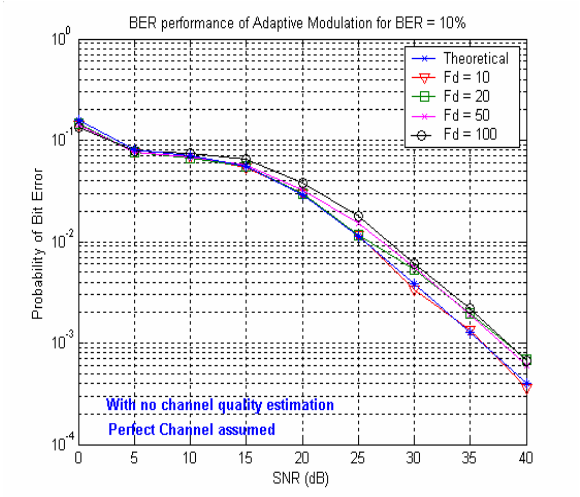

Figure 3.13 (a) BER performance of adaptive modulation with different Doppler frequency

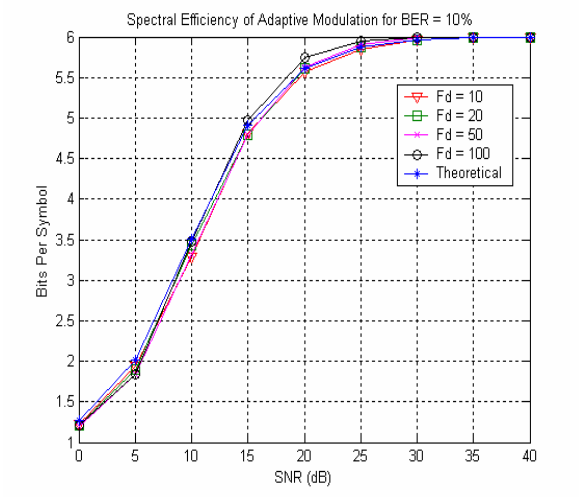

Figure 3.13 (b) Spectral efficiency of adaptive modulation with different Doppler frequency

BER = 1%

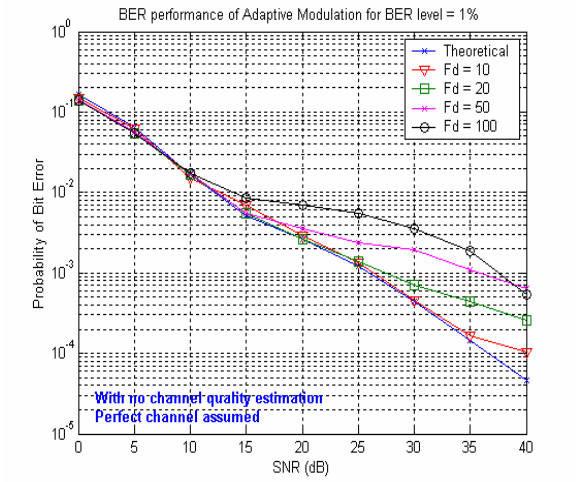

Figure 3.14 (a) BER performance of adaptive modulation with different Doppler frequency

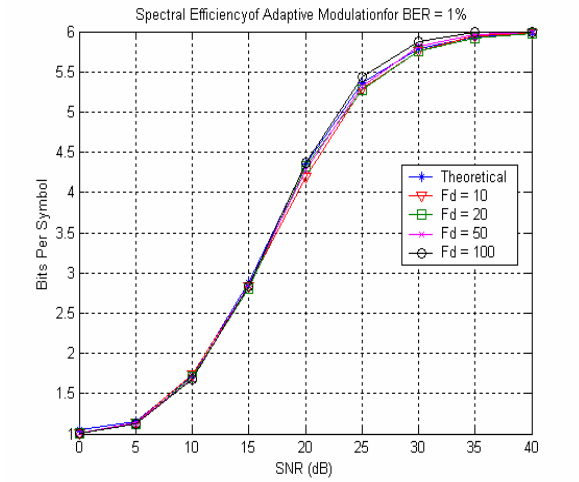

Figure 3.14 (b) Spectral efficiency of adaptive modulation with different Doppler frequency

3.4.4 Impact of channel equalization

We would now like to relax the restriction on perfect channel estimation and investigate the effect of the channel estimation and equalization[3] techniques discussed in Chapter 2 on the performance of adaptive modulation. In Chapter 2 we showed that for QAM modulation schemes, the FFT interpolator was superior to the Gaussian and Wiener interpolators. We would like to see how that transfers to adaptive modulation. In this section we specifically investigate the impact that the Gaussian and FFT interpolators have on the performance of adaptive modulation. Figure 3.15 shows the performance of adaptive modulation when using second order Gaussian interpolation. Here we consider the case of 0.1% BER target.

Table 3.5 Specifications used for the simulation results of Figures 3.15

Pilot symbol spacing	64
Doppler frequency	10Hz
Frame length	64 symbols
Symbol rate	32kHz
Frame duration	2ms

As discussed in Chapter 2 we expect an error floor in bit error rate performance when employing a Gaussian interpolator. Because of the error floor when employing Gaussian interpolation with QAM modulation, adaptive modulation suffers drastically at high values of SNR. As a result, we cannot achieve the target BER of 0.1%. Note that if a higher target were chosen, this error isn't as big of an issue as can be seen in Figures 3.15(c)-3.15(e). The spectral efficiency of adaptive modulation when using the Gaussian

[3] Note that by equalization we do not mean traditional equalization necessary in frequency selective channels where frequency equalization is performed. Rather, we mean time domain equalization since with QAM modulation, we must remove the amplitude variation induced by the channel as well as the phase variation.

interpolator is identical to the case of perfect channel estimation regardless of the target error rate. Again, this is expected since the spectral efficiency is only dependent on the channel statistics and the accuracy with which the channel quality is measured.

We now investigate the effect of the FFT channel estimator on the performance of adaptive modulation. As discussed in Chapter 2, FFT interpolation performs better than the Gaussian interpolator and Wiener interpolator and is our interpolator of choice. Figures 3.16 (a) and (b) show the impact of the FFT channel estimation technique on the performance of adaptive modulation along with different frame delays. Table 3.6 summarizes the parameters used in simulation results of Figures 3.16.

Table 3.6 Specifications used for the simulation results of Figures 3.16

Pilot symbol spacing	64
Doppler frequency	10Hz
Frame length	64 symbols
Symbol rate	32kHz
Frame duration	2ms

We note that without considering the impact of feedback delay, the FFT estimator introduces approximately 2-3dB of loss in the BER performance of adaptive modulation. The degradation increases for high values of average SNR (e.g., 5 dB at 25 dB average SNR), but the scheme still achieves the target BER value as the error floor is well beneath the target error rate. Since the target is achieved, the larger degradation at high SNRs may be irrelevant. We also examine the effect of feedback delay with FFT interpolation. As the feedback delay increases, the point at which the performance curve begins to flatten is at higher error rates. Thus, depending on the error rate target a lower delay value can be tolerated. In general, we can say that the Gaussian interpolator is

insufficient due its poor performance for QAM at high SNR values. The FFT approach however, is very promising and allows for good performance of adaptive modulation.

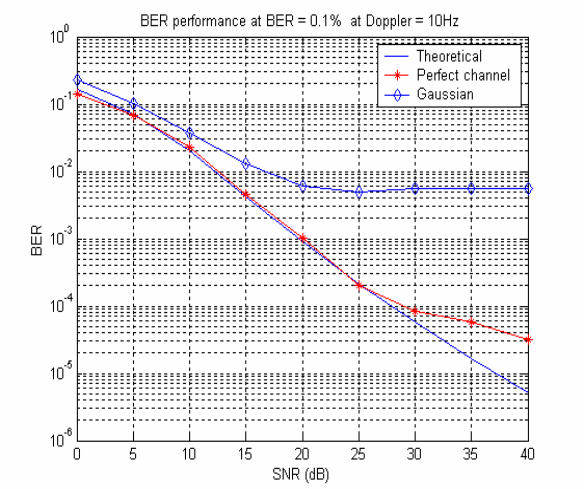

Figure 3.15(a) BER performance for the adaptive modulation with the Gaussian interpolator at BER = 0.1%

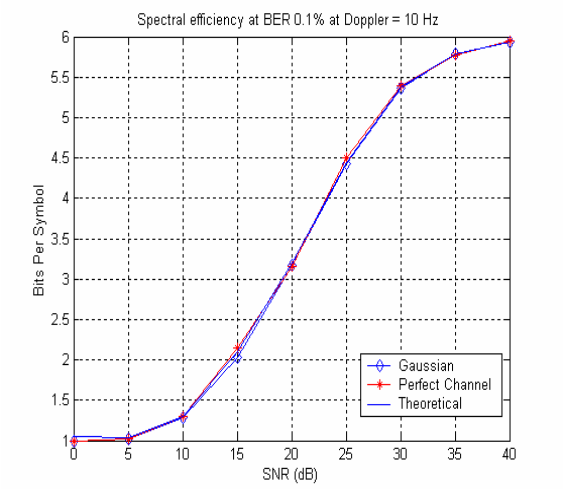

Figure 3.15(b) Spectral efficiency of the adaptive modulation with the Gaussian interpolator at BER = 0.1%

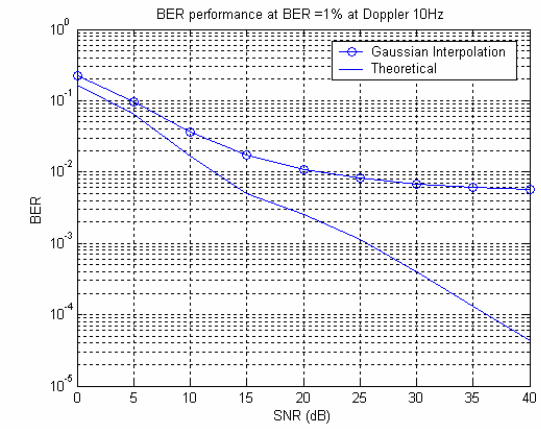

Figure 3.15(c) BER performance for the adaptive modulation with the Gaussian interpolator at BER =1%

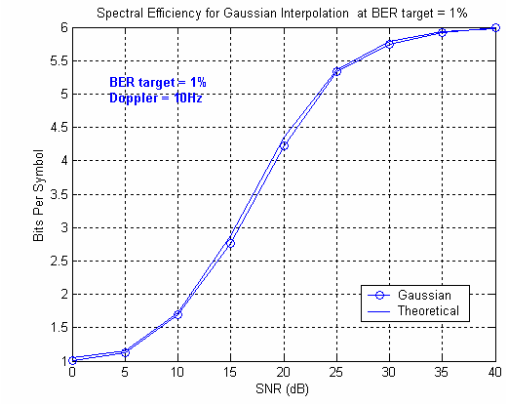

Figure 3.15(d) Spectral efficiency of the adaptive modulation with the Gaussian interpolator at BER =1%

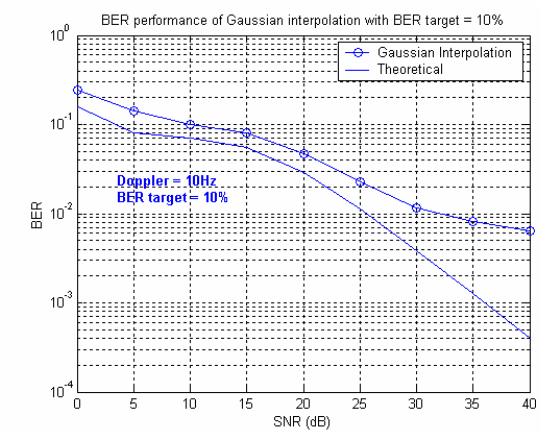

Figure 3.15(e) BER performance for the adaptive modulation with the Gaussian interpolator at BER =10%

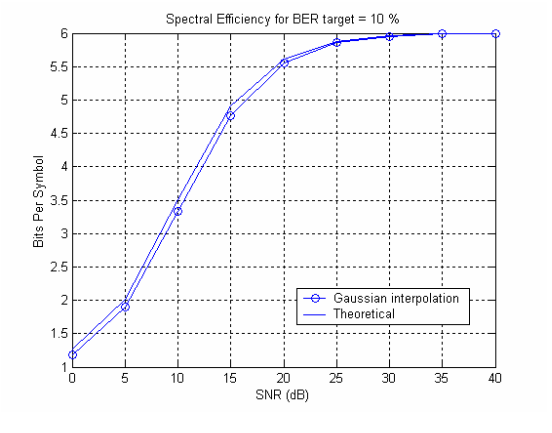

Figure 3.15(f) Spectral efficiency of the adaptive modulation with the Gaussian interpolator at BER =10%

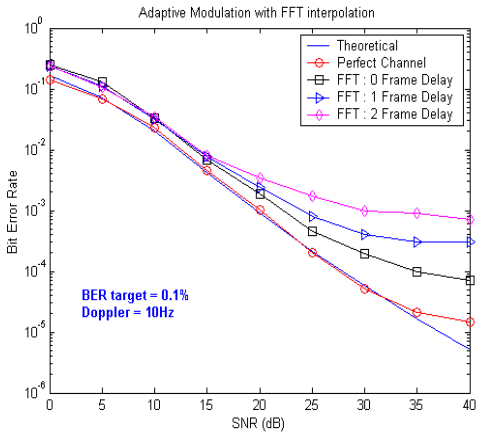

Figure 3.16 (a) BER performance of adaptive modulation with feedback delay for FFT interpolation at BER target = 0.1%

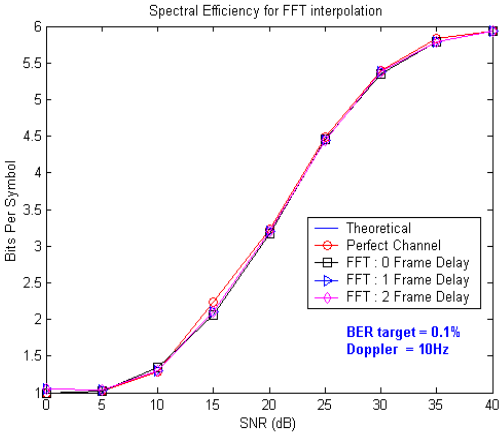

Figure 3.16 (b) Spectral efficiency of adaptive modulation with feedback delay for FFT interpolation at BER target = 0.1%

3.5 Chapter summary

In this chapter we examined the performance of adaptive modulation as proposed by Hanzo and Torrance under non-ideal conditions. We extended their work to include the impact of feedback delay, fading rate, and channel estimation techniques. We observed that high Doppler rates degrade the performance of adaptive modulation, even under ideal conditions. Further, when accounting for feedback delays, high Doppler rates were even more damaging. In terms of channel estimation, FFT interpolation significantly outperformed Gaussian interpolation and provided sufficient performance for adaptive modulation. In the next chapter we will investigate the impact of channel quality estimation as well as investigate long-term adaptation.

Chapter 4 ANALYSIS OF CHANNEL QUALITY (SNR) ESTIMATION ON ADAPTIVE MODULATION

4.1 Introduction

In the previous chapter we introduced and investigated the performance of adaptive modulation. The performance results assumed that the instantaneous channel SNR was known perfectly. In this chapter we investigate the impact of SNR or channel quality estimation on the performance of adaptive modulation. The adaptive modulation technique uses an estimate of the SNR at the receiver (which is reported to the transmitter via feedback) to choose a modulation scheme to obtain a given performance target. By adapting the modulation scheme, the link is able to improve the spectral efficiency as compared to static modulation. However, perfect knowledge of the SNR cannot be obtained, and thus there will be some error in the estimate.

We discuss SNR estimation techniques and their impact on the performance of adaptive modulation. Specifically, we examine two methods of estimating the channel SNR over a single frame. We will show that in channels with high Doppler spread, SNR estimation can be problematic and thus we propose an improved technique. Initially we shall assume perfect knowledge of the channel when such knowledge is required and then we will introduce channel estimation.

In channels with high to moderate Doppler, feedback delay can cause performance to degrade compared to theory as seen in the last chapter. This is especially true when channel estimation must be done as we will show. Thus, in the second half of this chapter we investigate long term SNR estimation which is not sensitive to feedback delay. We investigate the estimation accuracy and the performance of adaptive modulation when using long-term estimates to adapt the modulation scheme.

4.2 Channel Quality Estimation

The transmitter constantly needs information from the receiver in order to adapt the modulation scheme for the next active frame (Figure 3.1). The information provided by the receiver can be either the channel quality (allowing the transmitter to make rate decisions) or a selected modulation scheme. In either case, the modulation scheme chosen depends on an estimate of the channel quality at the receiver. Channel quality metrics include frame error rate, bit error rate, Viterbi decoder metrics, and SNR [14]. In this work we consider using SNR estimates as an indication of channel quality. Thus, the receiver requires a good SNR estimation technique to provide a reliable evaluation of the channel quality at the receiver. Ideally, a good SNR estimation technique should have the following properties:

- Independent of the Doppler frequency
- Independent of the modulation schemes
- Estimable using a small number of samples
- Provides an accurate channel quality estimate in both noise and interference limited conditions

However, we find that often we must sacrifice some of these properties for practical considerations. Let us assume that we have a complex baseband representation of the received signal samples given by

$$r_i = c_i d_i + n_i \tag{4.1}$$

where c_i is the received channel sample with variance $s^2 = SNR$ where SNR is the channel signal-to-noise ratio, d_i is the data symbol (with unit average energy), and n_i is additive white Gaussian noise. Each signal is complex and the variance of the noise *in the real and imaginary parts is* $s^2 = \frac{1}{2}$. Note that the total noise power is $s^2_{total} = 1$ [15], [16]. Let us represent the estimate of the received signal amplitude over a frame by Z and

the estimate of the noise variance by T^2. When Z and T^2 are calculated using the symbols of only one frame, we refer to this approach as "*Short Term SNR estimation*". The maximum likelihood estimate of SNR when using BPSK or QPSK modulation, assuming a constant channel SNR is [16]

$$\begin{aligned} \hat{g} &= \frac{|Z|^2}{T^2} \\ Z &= \frac{1}{N}\sum_{i=1}^{N} r_i d_i \\ &= \frac{1}{N}\sum_{i=1}^{N} a_i + n_i \\ T^2 &= \frac{1}{N-1}\sum_{i=1}^{N} (r_i d_i - Z)^2 \end{aligned} \tag{4.2}$$

It can be shown that $\hat{g}$ is the ratio of a non-central Chi-square random variable with ν_1=1 degree of freedom and a central Chi-square random variable with ν_2=*N-1* degrees of freedom [16]. Thus, it is well known that the random variable $\frac{n_1}{n_2}\hat{g}$ is a non-central *F*-distribution with ν_1 and ν_2 degrees of freedom and a non-centrality parameter λ=*N*γ [16], [17]. Using this estimate, we can now define the probability of using modulation scheme *k* as the probability that the SNR *estimate* $\hat{g}$ is between the levels associated with that scheme given that the true SNR is γ. That is we define:

$$\begin{aligned} P_{\text{mod}}(bpsk|g) &= \int_{l_1}^{l_2} p(\hat{g}|g)\,d\hat{g} \\ P_{\text{mod}}(qpsk|g) &= \int_{l_2}^{l_3} p(\hat{g}|g)\,d\hat{g} \\ P_{\text{mod}}(16qam|g) &= \int_{l_3}^{l_4} p(\hat{g}|g)\,d\hat{g} \\ P_{\text{mod}}(64qam|g) &= \int_{l_4}^{l_5} p(\hat{g}|g)\,d\hat{g} \end{aligned} \tag{4.3}$$

where $p\left(\hat{g}\middle|g\right)$ is the probability of the SNR estimate being $\hat{g}$ given that the SNR is γ. For perfect SNR estimation $p\left(\hat{g}\middle|g\right)=d\left(\hat{g}-g\right)$. However, when using the maximum likelihood estimate for SNR, the distribution is $F\left(\frac{N-1}{1}x\middle|1,N-1,Ng\right)$ where $F\left(x\middle|n_1,n_2,l\right)$ is the non-central *F*-distribution with ν_1 and ν_2 degrees of freedom and non-centrality parameter λ [16], [17]:

$$F\left(x\middle|n_1,n_2,l\right)=\sum_{i=0}^{\infty}e^{-l/2}\frac{\left(l/2\right)^i}{i!}\frac{\left(n_1+2i\right)^{\frac{n_1+2i}{2}}}{B\left(\frac{n_1+2i}{2},\frac{n_2}{2}\right)}x^{\frac{n_1+2i-2}{2}}\left(n_2+\left(n_1+2i\right)x\right)^{-(n_1+2i+n_2)/2} \quad (4.4)$$

where *B(a,b)* is the standard complete beta function [17]. Unfortunately, the above distribution is difficult to compute for large values of λ and *i* due to combined overflow and underflow problems. Thus, for computation we shall rely on an approximation using the standard normal distribution. It is given as [17]:

$$\begin{aligned}&F\left(x\middle|n_1,n_2,l\right)\approx P(x_2)\\&x_2=\frac{\left[\frac{n_1x}{n_1+l}\right]^{1/3}\left[1-\frac{2}{9n_2}\right]-\left[1-\frac{2\left(n_1+2l\right)}{9\left(n_1+l\right)}\right]}{\left[\frac{2}{9}\frac{n_1+2l}{\left(n_1+l\right)^2}+\frac{2}{9n_2}\left(\frac{n_1}{n_1+l}x\right)^{2/3}\right]^{1/2}}\end{aligned} \quad (4.5)$$

where *P(x)* is the standard normal distribution. The probability of error in this case is given by

$$P_e\left(\Gamma\right)=\frac{1}{B}\left[\begin{aligned}&1\int_0^{\infty}P_{\mathrm{mod}}\left(bpsk\middle|g\right)P_{bpsk}\left(g\right)f\left(g\middle|\Gamma\right)dg+2\int_0^{\infty}P_{\mathrm{mod}}\left(qpsk\middle|g\right)P_{qpsk}\left(g\middle|\Gamma\right)f\left(g\right)dg\ldots\\&+4\int_0^{\infty}P_{\mathrm{mod}}\left(16qam\middle|g\right)P_{16qam}\left(g\middle|\Gamma\right)f\left(g\right)dg+6\int_0^{\infty}P_{\mathrm{mod}}\left(64qam\middle|g\right)P_{64qam}\left(g\middle|\Gamma\right)f\left(g\right)dg\end{aligned}\right]$$

where Γ is the average SNR and $P_{scheme}(g)$ is the probability of error for modulation technique *scheme.*

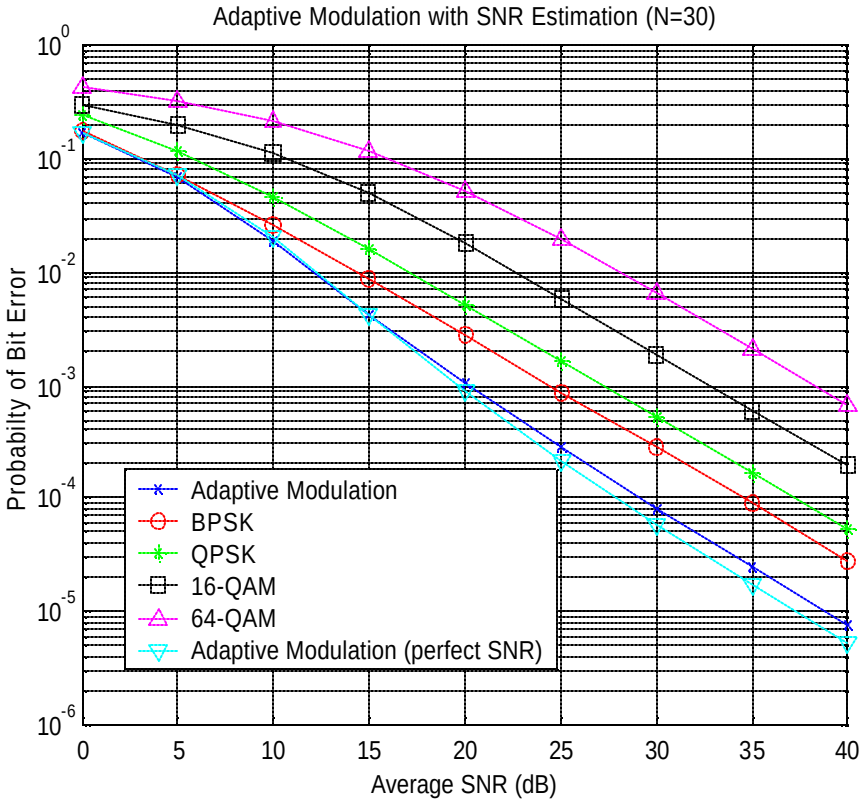

Figure 4.1 Performance of Static and Adaptive Modulation with Perfect and Estimated SNR (N = 32)

Figure 4.1 presents the performance of adaptive modulation with perfect SNR estimation and maximum likelihood estimation with N=32 for a target error rate of 0.1%. We can see that with 32 symbols to estimate the SNR, the estimation does not significantly impact the performance. However, this assumed perfect knowledge of the symbols. With estimation or eliminating the modulation, the estimation may have more of an impact.

It can be shown that the above estimator for SNR is biased. An unbiased estimate of SNR can be calculated as [18]:

$$\hat{\Gamma}_{short} = \left(\frac{N-3}{N-1}\right)\frac{|Z|^2}{T^2} - \frac{1}{N} \tag{4.6}$$

Additionally, the above estimator requires knowledge of the data symbols d_i. Since we shall use BPSK/QPSK in low SNR conditions, we would like an estimator that does not depend on the estimate of the data symbol. Thus, we shall use a modified form of the unbiased ML estimator:

$$\hat{g} = \left(\frac{N-3}{N-1}\right)\frac{|Z|^2}{T^2} - \frac{1}{N}$$
$$Z = \frac{1}{N}\sum_{i=1}^{N}|r_i|$$
$$T^2 = \frac{1}{N-1}\sum_{i=1}^{N}\left(|r_i| - Z\right)^2$$

Of course these estimators are to be applied to constant modulus modulation schemes. For QAM we use:

$$\hat{g} = \left(\frac{N-3}{N-1}\right)\frac{|Z|^2}{T^2} - \frac{1}{N}$$
$$Z = \frac{1}{N}\sum_{i=1}^{N}\frac{r_i}{d_i} \tag{4.7}$$
$$T^2 = \frac{1}{N-1}\sum_{i=1}^{N}\left(|r_i - Zd_i|\right)^2$$

which will clearly require symbol estimates. This is unavoidable since the modulation scheme introduces amplitude variations. We shall use the term “conventional” to represent this short-term SNR estimation technique. Figures 3.3 through 3.6 show the theoretical results of the short term SNR with perfect SNR estimation and BER targets of 0.1%, 1% and 10%. The SNR ranges corresponding to the three different BER levels are described in Table 4.1.

4.3 Impact of Short term SNR estimation on adaptive modulation

As discussed, the SNR estimate is fed to the transmitter, which is used to choose the modulation scheme for the next active frame. The main advantage of adaptive modulation is that it works well in slow fading channel, meaning that the channel variation over one frame is considered to be nearly constant. As a result, estimating the channel SNR from one frame's worth of symbols should give us an accurate estimate of the SNR for the next frame.

Table 4.1 Summarizes the conditions on the estimated SNR

Conditions on estimated SNR	**Modulation adapted**
BER = 10%	
SNR<= 2dB	BPSK
2dB<SNR<=8dB	QPSK
8dB<SNR<=12dB	16QAM
12dB<SNR<=40dB	64QAM
BER = 1%	
SNR<= 8dB	BPSK
8dB<SNR<=14dB	QPSK
14dB<SNR<=20dB	16QAM
20dB<SNR<=40dB	64QAM
BER = 0.1%	
SNR<= 11dB	BPSK
11dB<SNR<=17dB	QPSK
17dB<SNR<=25dB	16QAM
25dB<SNR<=40dB	64QAM

Figures 4.2 (a) and (b) provide a comparison of short-term adaptation at 5Hz with and without perfect knowledge of channel SNR. Table 4.2 summarizes the parameters used for the simulation results of Figures 4.2.

Table 4.2 Specifications used for the simulation results of Figures 4.2

Pilot symbol spacing	64
Doppler frequency	5Hz
Frame length	64 symbols
Frame rate	500Hz
Symbol rate	32kHz
Frame duration	2ms

As seen in Figure 4.2, at Dopplers as low as 5Hz, adaptive modulation using estimated channel SNR values performs nearly as well as in the case of the perfect knowledge of channel SNR. This is in agreement with our predicted performance results shown in Figure 4.1. Thus, despite the fact that we have changed the estimator slightly, using the modified ML estimate rather than the ML estimate, the performance matches theory well. At 5Hz Doppler, a frame rate of 500Hz and with 64 symbols to estimate the SNR, we can achieve performance nearly identical to theoretical performance with perfect SNR knowledge.

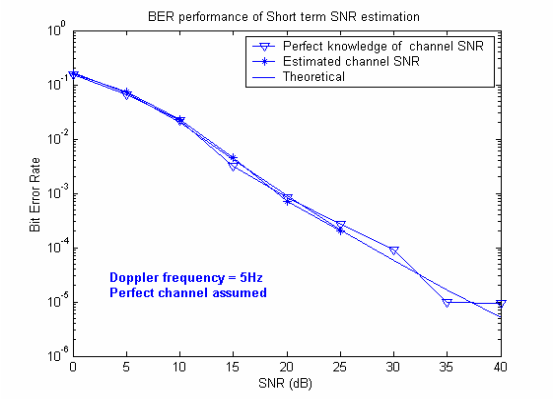

Figure 4.2 (a) BER performance of Adaptive Modulation with short term SNR estimation at Doppler 5Hz with and without the perfect knowledge of channel SNR

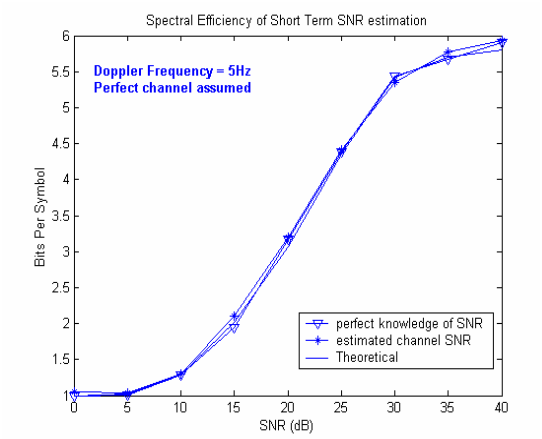

Figure 4.2 (b) Spectral efficiency of Adaptive Modulation with short term SNR estimation at Doppler 5Hz with and without the perfect knowledge of channel SNR

The previous example considered a slow fading case. In Figure 4.3, we examine the performance of adaptive modulation with short-term SNR estimation in the presence of higher Doppler spreads. We observe that at a Doppler frequency of 10Hz and up, there is a slight degradation in both BER performance and spectral efficiency. The reduction in spectral efficiency is directly related to the accuracy in the SNR estimate. A plot of estimated vs. true SNR is shown in Figure 4.5 (a) for a Doppler rate of 50Hz. It can be seen that at high to moderate Doppler frequencies, there is significant deviation in the estimated SNR from the true SNR. This is because as the Doppler frequency increases, the channel changes more rapidly, and therefore the channel doesn't remain constant over a frame. As a result, the variance estimate is impacted by the channel variation. This puts a lower limit on the noise variance estimate and a resulting ceiling on the SNR estimate as seen in Figure 4.5 (a). This results in an underestimation of the SNR in many cases. The reduced SNR estimate means that BPSK and QPSK will be used more often than desired and the resulting spectral efficiency will be significantly reduced. The impact that Doppler spread has on the BER performance is slightly more complicated. As seen in Chapter 3, an increase in Doppler spread degrades the performance of adaptive modulation with perfect SNR estimation. This is because the channel changes during a

frame and the chosen modulation scheme is no longer optimal. With SNR estimation, using BPSK and QPSK more often then desired will actually improve BER perfromacne while hurting spectral efficiency. The net result of these two effects is still a net reduction in the performance as compared to slow fading rates. Table 4.3 summarizes the frame rate used in Figures 4.3 where F_d is the Doppler rate and T_f is the frame duration.

Table 4.3 Relationship between Frame Rate and Doppler rate for Simulations in Figure 4.3

Dopplers	**Frame Rate**	**F_d*T_f**
5Hz	500	0.01
10Hz	500	0.02
50Hz	500	0.1
100Hz	500	0.2

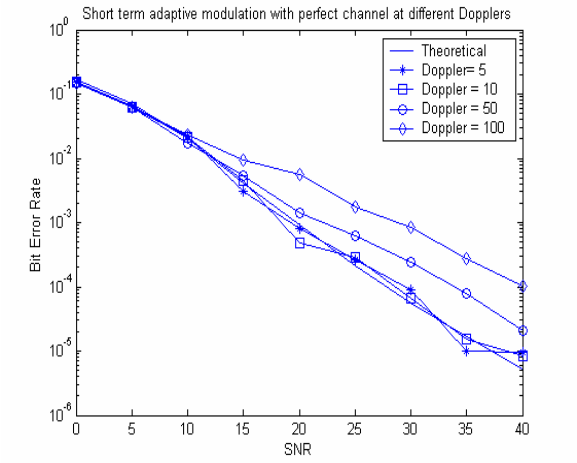

Figure 4.3 (a) BER performance of Adaptive Modulation with short term SNR estimation at different Dopplers of at a BER target of 0.1%

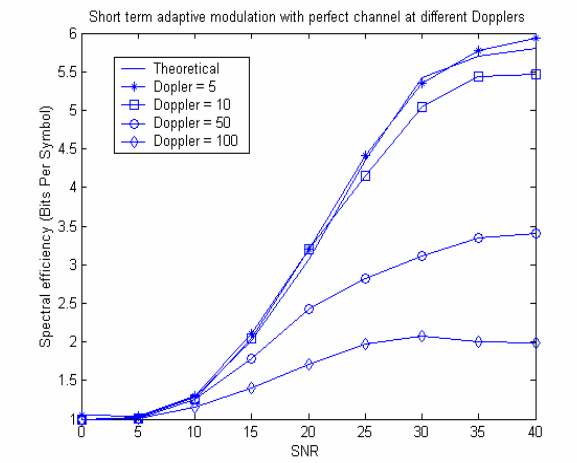

Figure 4.3 (b) Spectral efficiency of Adaptive Modulation with short term SNR estimation at different Dopplers at a BER target of 0.1%

Thus, in order to improve the performance of adaptive modulation in moderate to high Doppler spreads we must improve the estimate of the noise power. In order to reduce the effect of channel variation on the noise power estimate, we propose the use of channel estimates in the noise power calculation instead of using the mean value of the channel. That is we use

$$T^2 = \frac{1}{N-1}\sum_{i=1}^{N}\left(|r_i| - |\hat{c}_i|\right)^2$$
$$T^2 = \frac{1}{N-1}\sum_{i=1}^{N}\left(|r_i - \hat{c}_i d_i|\right)^2 \qquad (4.8)$$

for the noise power estimates for PSK and QAM respectively. We term this technique "*Improved short term SNR estimation*". We use the improved scheme for the short term SNR estimation in order to compensate for the channel variation at high Doppler rates.

Figure 4.5 (b) shows the SNR estimate with the improved short term SNR estimation at a Doppler spread of 50Hz. Note the improvement in SNR estimation at high SNR values seen in Figures 4.5(a) and 4.5(b). Figures 4.4 (b) and 4.6 (b) show how the spectral efficiency is affected by the SNR estimation technique at Doppler rates of 5Hz and 50Hz. We can see that at slow Doppler rates, there is no difference in BER performance or spectral efficiency when using the two estimation techniques. However, at higher Doppler rates, we see that there is a significant improvement in spectral efficiency when using the improved SNR estimation technique. As seen in Figure 4.5 the SNR estimate is drastically improved leading to a proper choice of modulation scheme and corresponding higher spectral efficiency. Unfortunately, this actually degrades BER performance which is expected by examining the performance with perfect SNR knowledge. At high Doppler rates, adaptive modulation suffers even with perfect SNR knowledge since adaptation is not sufficiently fast.

Perfect Channel , BER level = 0.1%, Doppler = 5Hz

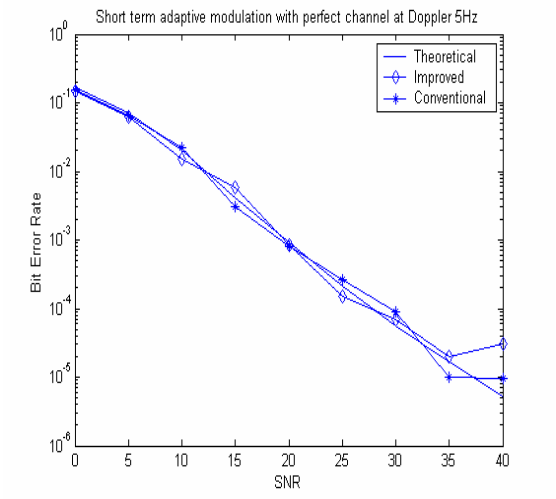

Figure 4.4 (a) BER performance for the short term SNR estimation at low Doppler of 5Hz at BER target of 0.1%

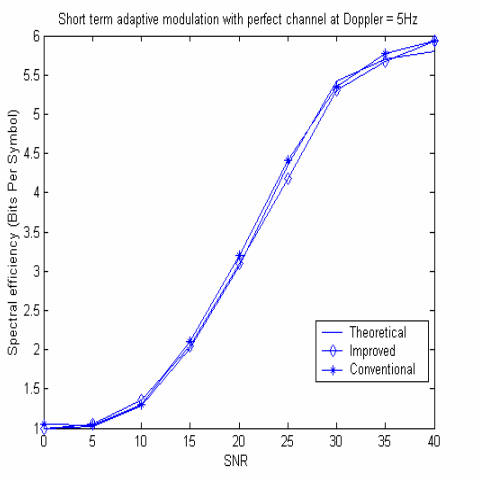

Figure 4.4 (b) Spectral efficiency for the short term SNR estimation at low Doppler of 5Hz

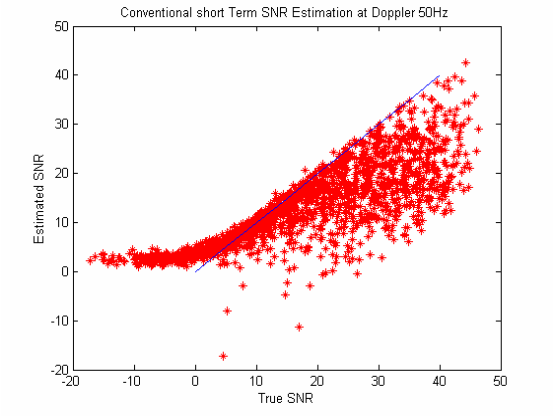

Figure 4.5 (a) Estimated vs. True SNR performance for the short term SNR estimation at Doppler 50Hz

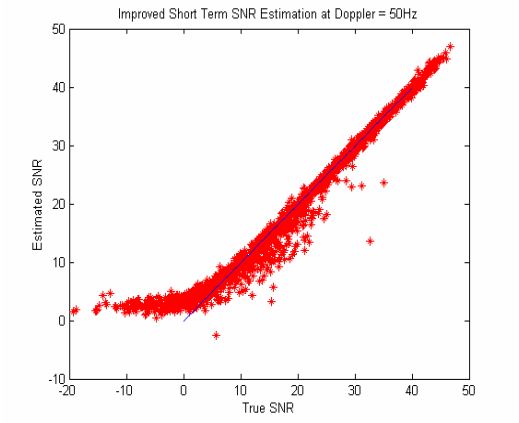

Figure 4.5 (b) Estimated vs. True SNR performance for the Improved short term SNR estimation at Doppler 50Hz

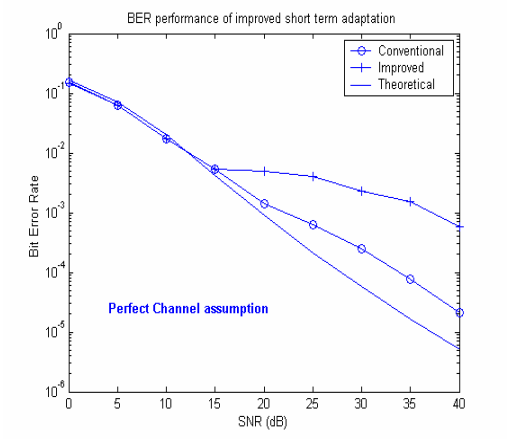

Figure 4.6 (a) BER performance for the short term SNR estimation at Doppler 50Hz

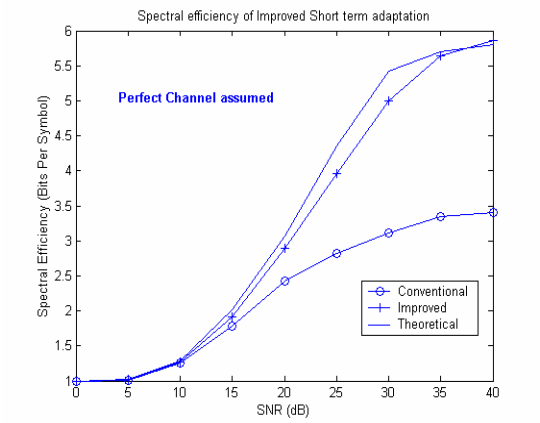

Figure 4.6 (b) Spectral efficiency for the short term SNR estimation at Doppler 50Hz

In adaptive modulation, our main goal is to achieve higher spectral efficiency without significantly affecting the bit error. The remainder of our simulation results of adaptive modulation will focus on a BER target of 0.1% with improved short term SNR estimation method.

4.4 Impact of SNR Estimation on Adaptive Modulation with FFT channel estimation

Up to this point we have assumed perfect channel estimation and equalization. We now present results for adaptive modulation with both short term SNR estimation and FFT channel interpolation Figure 4.7 presents results for adaptive modulation at a Doppler rate of 5Hz and 50Hz for both SNR estimation techniques. We observe that at a Doppler rate of 5Hz, performance of adaptive modulation with conventional and improved Short term SNR estimation remains almost same, however, at 50 Hz, when using FFT interpolation with improved short term SNR estimation spectral efficiency degrades and in comparison to the conventional method, there is no improvement in spectral efficiency of Improved method over the conventional short term SNR estimation technique. This is directly due to the channel estimation.

We recall from Chapter 2 that FFT interpolation causes edge effects which impact the channel estimation at the edge frames. The impact of this can be avoided in the demodulation process by introducing a delay in demodulation (i.e., demodulating the middle frame of the channel estimation region). However, as we have seen, delays cannot be tolerated in adaptive modulation especially in high Doppler situations. Thus, we must use the edge frame to estimate the SNR to avoid delays in SNR estimation. Thus, degradation in the performance is experienced because the edge effect causes variation in the channel estimate which again puts a floor on the noise power estimate.

Short Term SNR estimation, FFT Interpolation

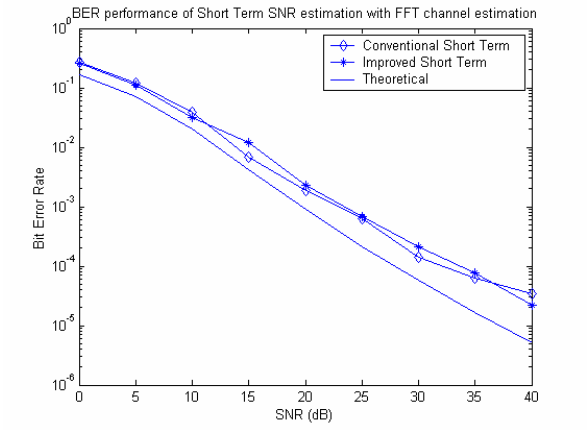

Figure 4.7 (a) BER performance for the short term SNR estimation at Doppler 5Hz .

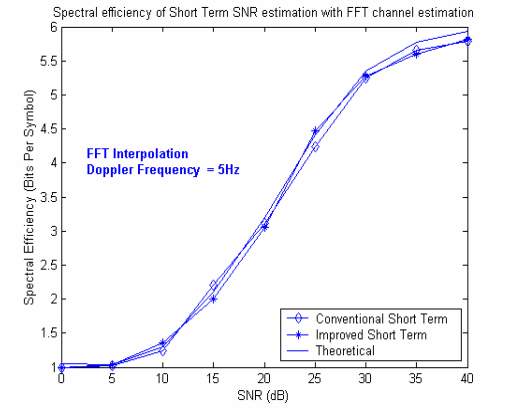

Figure 4.7 (b) Spectral efficiency at Doppler 5Hz

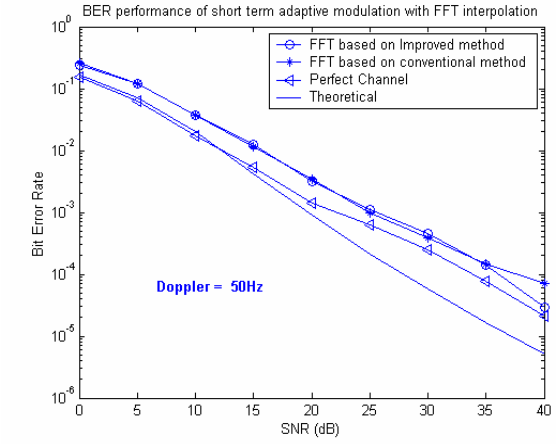

Figure 4.7 (c) BER performance for the short term SNR estimation at Doppler 50Hz.

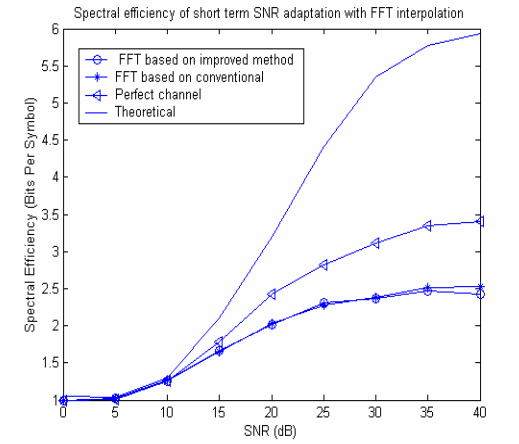

Figure 4.7 (d) Spectral efficiency at Doppler 50Hz

This leads us to propose in section 4.7, improved long term SNR estimation which is insensitive to delay, although it provides a less than optimal trade-off between energy and bandwidth efficiency than short term estimation and adaptation.

4.5 Impact of symbol decisions on the Improved short-term SNR estimation

Finally, in this section we shall examine the effect of the symbol estimation error on the performance of adaptive modulation. We observed in equation (4.7), we require an estimate of the transmitted symbol in order to estimate the channel SNR with QAM modulation schemes. We could either only use pilot symbols to estimate SNR or we can estimate all of the symbols. Since there is only one pilot symbol per frame, the former technique is not practical. Thus, we would like to determine the impact of symbol estimation error on the performance of adaptive modulation through SNR estimation. In Figure 4.8 we present simulation results for 50Hz Doppler spread and a target BER of 0.1% with FFT channel estimation. We plot the performance of adaptive modulation with and without perfect knowledge of the symbols when estimating SNR for QAM modulation. We can see that the symbol estimates required for SNR estimates (when QAM modulation is used) do not have a significant impact on performance.

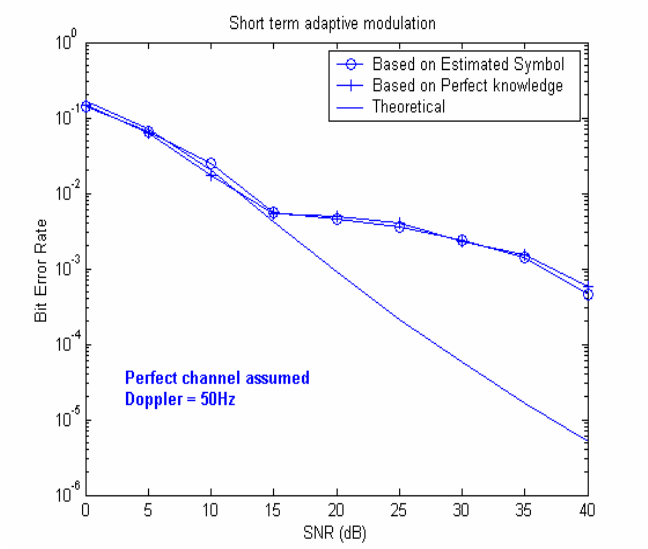

Figure 4.8 (a) BER performance for the short term SNR estimation at Doppler 50Hz

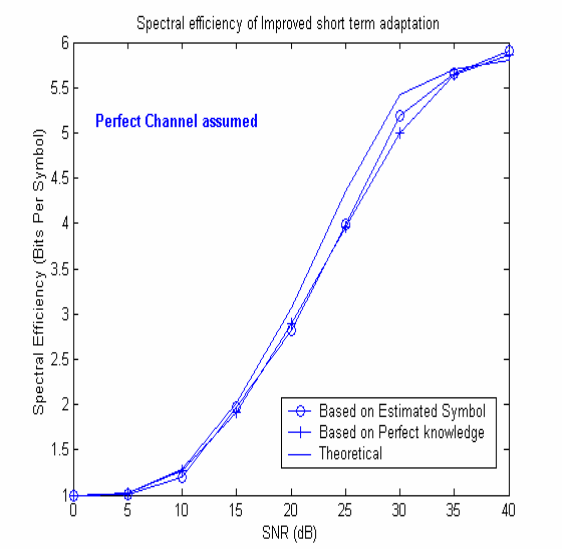

Figure 4.8 (b) Spectral efficiency for the short term SNR estimation at Doppler 50Hz

4.6 Analysis of long term SNR estimation

Up to this point we have discussed short term and improved short term SNR estimation. By introducing improved short term SNR estimation, we are able to solve the problem of SNR estimation in fast fading channels. However, when using FFT interpolation, improved short term SNR estimation isn't effective due to the edge effects and the intolerance of adaptive modulation to delay.

As an alternative approach, we examine the calculation of channel SNR over a long period of time. Such an approach would not provide as substantial an improvement in bandwidth efficiency, but it would be insensitive to delay. Such an approach would estimate *average SNR* over a longer window. This average SNR value can then be used to adapt the modulation scheme. Such an approach has the drawback that we can only adapt to long term changes in the channel SNR (e.g., changes to do shadowing or path loss). However, this approach would be a more accurate estimate of SNR since it would use more data for the estimation. Further,

we will show that the approach is more resistant to Doppler spread and feedback delay. Thus we propose and examine the use of *"Improved long term SNR estimation*".

As shown, the performance of adaptive modulation depends how well the channel SNR has been estimated. The more accurate the estimation of the channel SNR is, the better the choice of modulation will be, and the better the ability to handle the variations in the channel will be. This leads us to propose improved long term SNR estimation where SNR is calculated by averaging signal power and noise power over several frames. Thus, unlike short term SNR estimation, we are using symbols of more frames to calculate the signal power and noise variance. Also, instead of trying to estimate *instantaneous* SNR we are estimating average SNR over a certain window. For long-term estimation the SNR is calculated using the same equations as in the case of short term SNR estimation. However we now use the following long term estimates of channel amplitude and noise power:

$$\begin{aligned} Z_{long}(n) &= 0.99 Z_{long}(n-1) + 0.01 Z(n) \\ T^2_{long}(n) &= 0.99 T^2_{long}(n-1) + 0.01 T^2(n) \end{aligned} \tag{4.9}$$

where $Z(n)$ and $T^2(n)$ are calculated using the current frame consistent with the previously presented short term estimates. The long term SNR estimate is then calculated as

$$\hat{\Gamma}_{long} = \left(\frac{N-3}{N-1} \right) \frac{\left| Z_{long} \right|^2}{T^2_{long}} - \frac{1}{N} \tag{4.10}$$

Table 4.4 Summary of Switching Levels

Conditions on estimated SNR	Modulation adapted
BER = 10%	
SNR<= 5dB	BPSK
5dB<SNR<=10dB	QPSK
10dB<SNR<=15dB	16QAM
15dB<SNR<=40dB	64QAM
BER = 1%	
SNR<= 16dB	BPSK
16dB<SNR<=22dB	QPSK
22dB<SNR<=29dB	16QAM
29dB<SNR<=40dB	64QAM
BER = 0.1%	
SNR<= 27dB	BPSK
27dB<SNR<=32.5dB	QPSK
32.5dB<SNR<=37.5dB	16QAM
37.5dB<SNR<=40dB	64QAM

Note that since we are estimating the *average SNR* over a particular window, our choice of switching levels must account for the SNR variation. Thus, instead of using AWGN performance to choose our switching levels, we must use Rayleigh fading curves to choose switching levels as shown in Figure 4.9 (a) and Table 4.4. Figure 4.9s (b) through (e) provide the theoretical results of conventional long term SNR estimation for target error rates of 0.1%, 1% and 10% respectively using the switching levels given in Table 4.4..

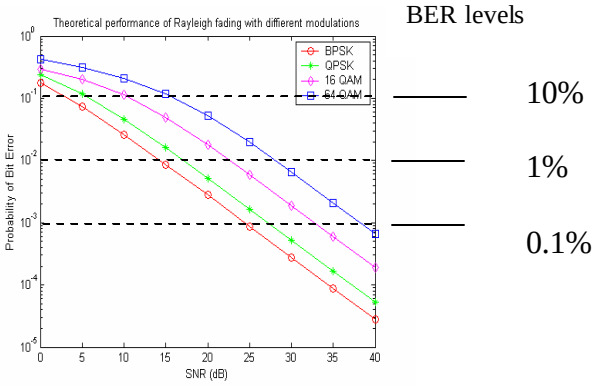

Figure 4.9(a) Theoretical BER performance of different modulation schemes in Rayleigh fading

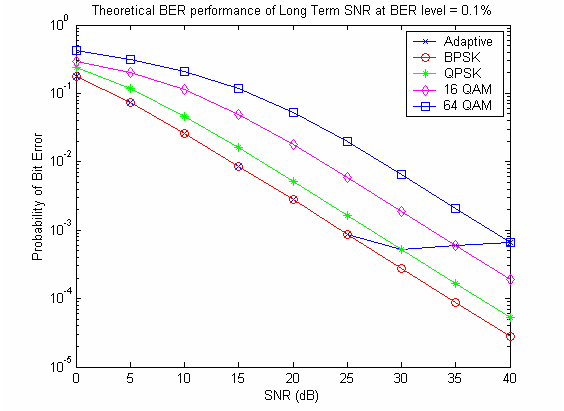

Figure 4.9(b) Theoretical BER performance of adaptive modulation with perfect long term SNR estimation for BER target of 0.1 %

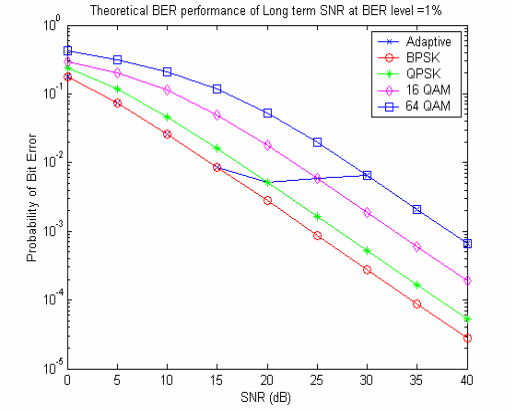

Figure 4.9(c) Theoretical BER performance of adaptive modulation with perfect long term SNR estimation for BER target of 1 %

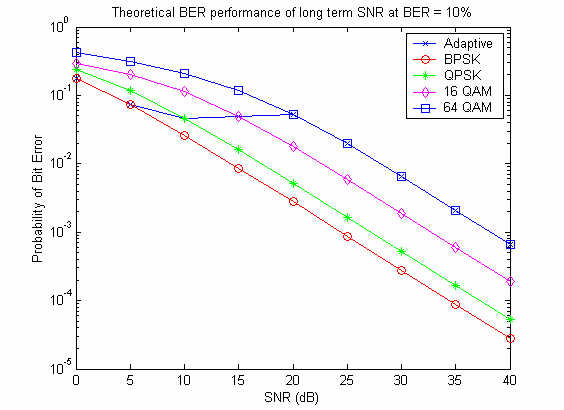

Figure 4.9(d) Theoretical BER performance of adaptive modulation with perfect long term SNR estimation for BER target 10 %

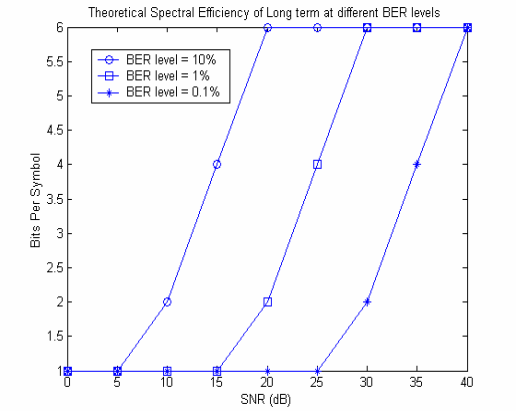

Figure 4.9(e) Spectral efficiency of adaptive modulation with perfect long term SNR estimation for all BER targets

We first examine the performance of long term SNR estimation using the conventional short term estimates of channel amplitude and noise power as given previously. Figure 4.10 shows the bit error rate performance and spectral efficiency at frequencies as low as 5Hz to as high as 50Hz. We notice that as the Doppler frequency increases, there is a degradation in the spectral efficiency which becomes more prominent at high frequency such as 50Hz. This is similar to the effect seen in short term estimation and stems from the same limitations in the noise power estimate. This can be seen in Figures 4.11(a) and 4.11(c). The long term SNR estimate is clearly limited at high SNRs due to the channel variation.

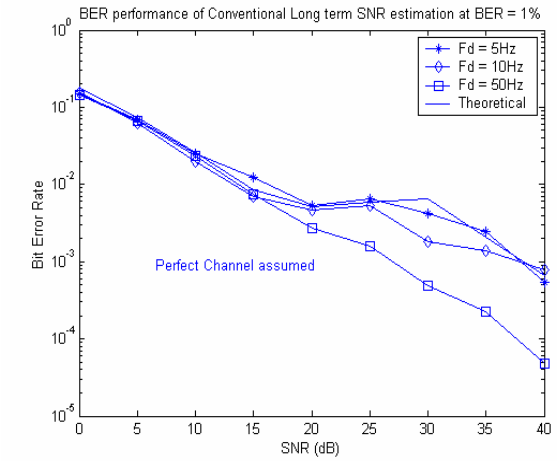

Figure 4.10 (a) BER performance of conventional Long term SNR estimation for BER target of 1 %.

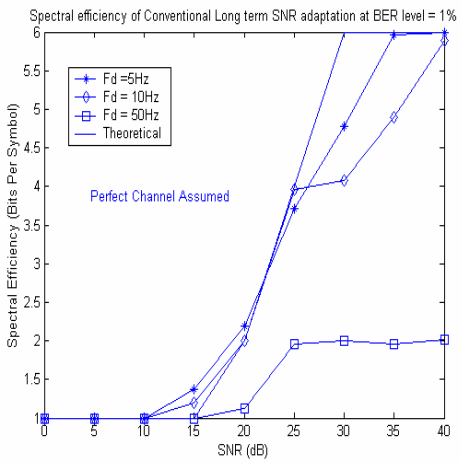

Figure 4.10 (b) Spectral Efficiency of conventional Long term SNR estimation for BER target of 1 %.

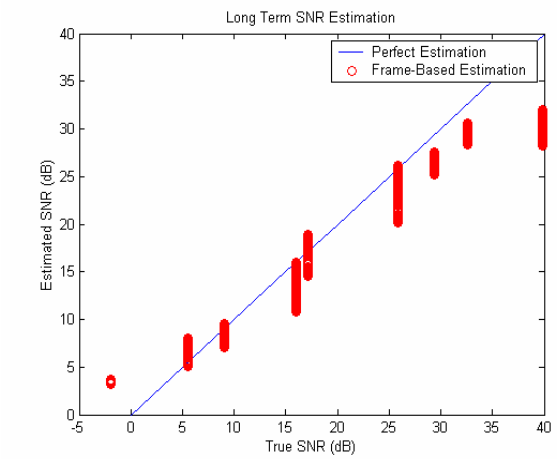

Figure 4.11 (a) Conventional Long term SNR estimation at Fd = 10Hz for BER target of 1 %.

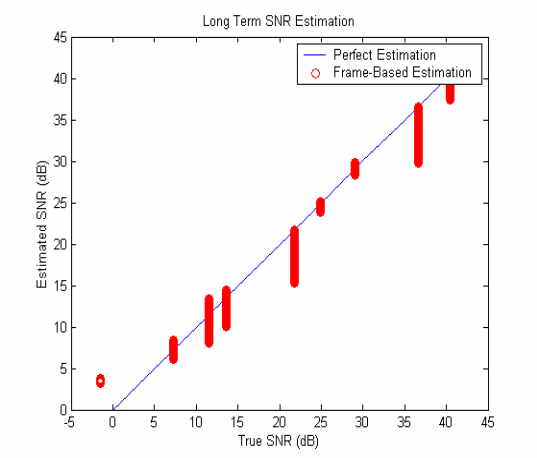

Figure 4.11 (b) Improved Long term SNR estimation at Fd = 10Hz for BER target of 1 %.

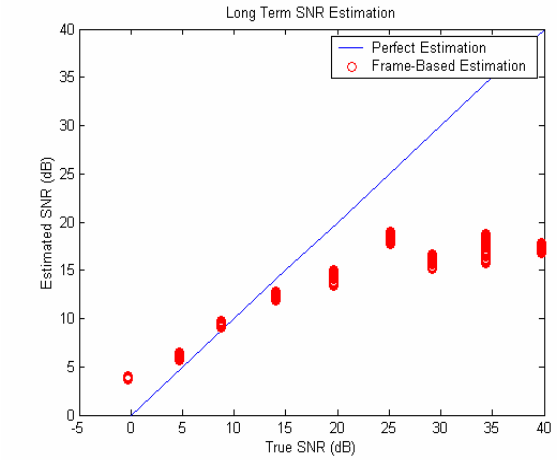

Figure 4.11 (c) Conventional Long term SNR estimation at Fd = 50Hz for BER target of 1 %.

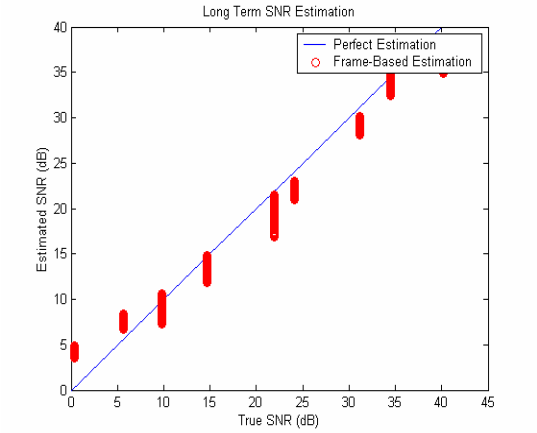

Figure 4.11 (d) Improved Long term SNR estimation at Fd = 50Hz for BER target of 1 %.

Figures 4.11(a) and (c) show that as the Doppler frequency increases, the estimated SNR vs. the true SNR loses the desired linear relationship. This is due to the channel variation at high to moderate Doppler values which impacts the noise power estimate as discussed previously. Again, to account for this variation, we propose an "improved" long term SNR estimation. This proposed method of long term SNR uses the channel estimates to estimate the noise power just as in the case of improved short term estimation. We

simply replace the estimate of $T^2(n)$ in equation (4.9) with the improved variance estimate given in equation (4.8). Figure 4.11 (b) and (d) shows that improved long term SNR estimation at Doppler frequencies provides significantly improved SNR estimation at10Hz and 50Hz respectively.

Figure 4.12 shows the effect of conventional long term SNR estimation vs. improved long term SNR estimation with perfect channel assumption at a Doppler frequency of 50Hz. We can see that the improved SNR estimate provides better spectral efficiency as was the case in short term estimation.

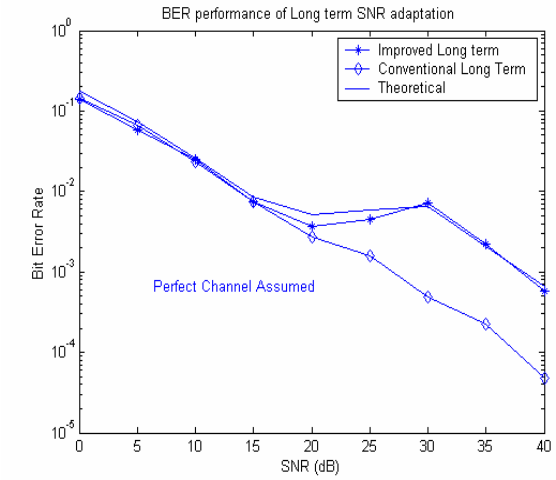

Figure 4.12 (a) BER performance of long term SNR estimation at BER target 1% with Doppler = 50Hz

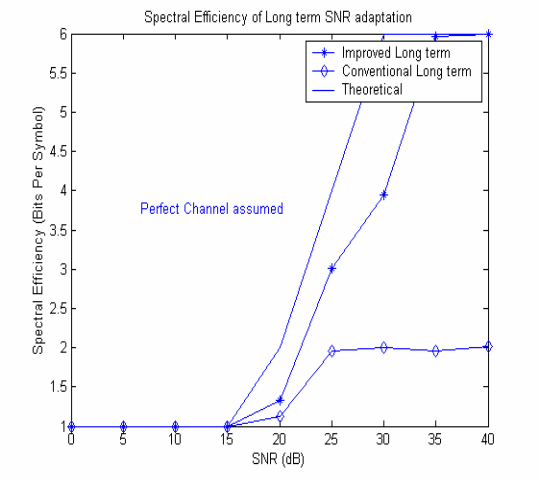

Figure 4.12 (b) Spectral efficiency of long term SNR estimation at BER target 1 % with Doppler = 50Hz

We observe that at 30dB, we get 4 bits per symbol from improved estimation whereas conventional is able to deliver only 2 bits per symbol.

4.7 Simulation results and discussion of long term SNR estimation

4.7.1 Effect of feedback delays

As discussed earlier, SNR estimates of the channel are provided through a feedback loop from the receiver to the transmitter. Necessarily, there will be some delay in transmitting this information back to the transmitter. We use the term feedback delay or frame delay to represent the number of frames between the time that SNR is estimated and the time that the modulation scheme is adapted based on that estimate. Figures 4.13(a) – (d) show the effect of frame delay results of improved long term SNR estimation with perfect channel and FFT interpolation.

Table 4.5 Specifications used for the simulation results of Figures 4.13

Pilot symbol spacing	64
Doppler frequency	10Hz
Frame rate	500Hz
Frame length	64 symbols
Symbol rate	32kHz
Frame duration	2ms

In the presence of FFT interpolation, improved long-term adaptation performs nearly as well as with perfect channel estimation. Additionally, spectral efficiency and bit error rate are insensitive to feedback delay. This is in contrast to the performance of short term adaptation where BER degradation increases with increasing delay. In Figure 4.13(a), we find that by employing improved long term SNR estimation, the bit error rate

performance doesn't degrade with feedback delays. Therefore, improved long term SNR estimation is more resistant to feedback delays.

BER = 1%; Perfect channel assumed, Improved Long Term SNR estimation

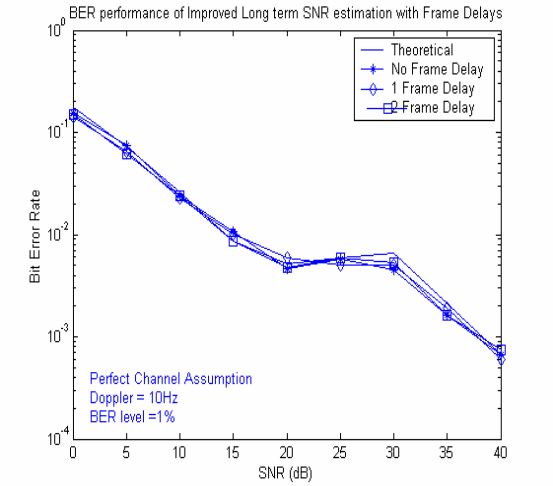

Figure 4.13 (a) BER performance of long term adaptive modulation at Doppler = 10Hz

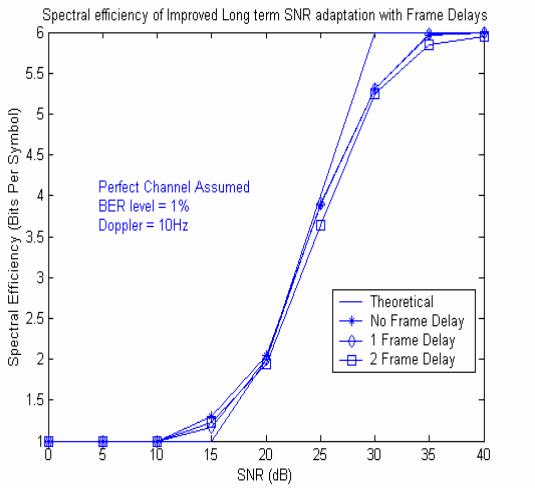

Figure 4.13 (b) Spectral efficiency of long term adaptive modulation

BER = 1%; FFT interpolation, Improved Long Term SNR estimation

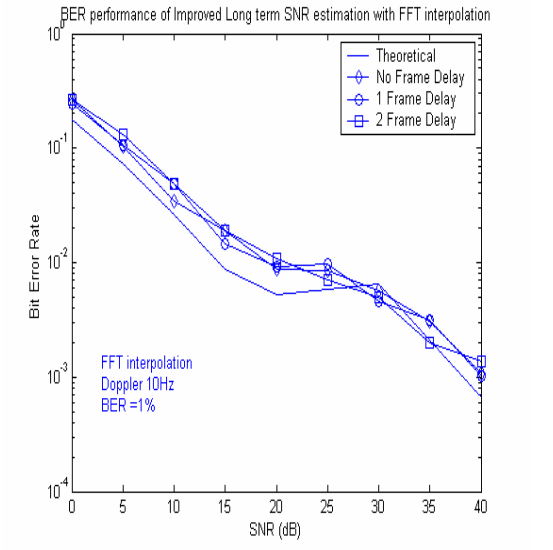

Figure 4.13 (c) BER performance of long term adaptive modulation

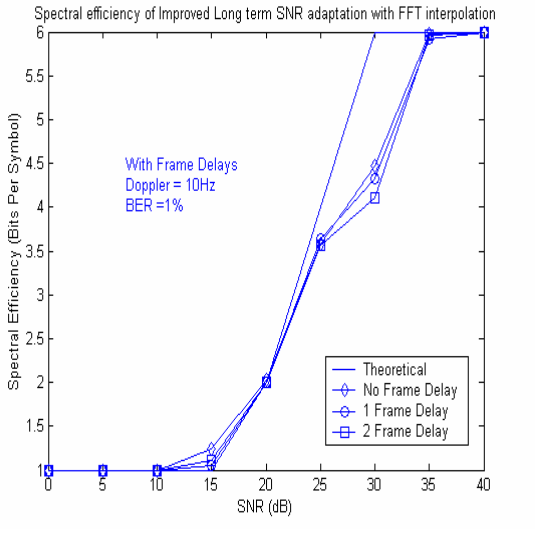

Figure 4.13(d) Spectral efficiency of long term adaptive modulation

Since there is a delay in implementing the estimated modulation for the right frame, we would expect degradation in the performance of adaptive modulation. However, improved long term SNR estimation does not attempt to keep up with short term changes. Therefore, improved long term SNR estimation is a practical technique when taking into account delay, Doppler spread and channel estimation. Since in reality, there would be significant delay in transmitting information of modulation from the receiver to the transmitter, using the proposed method of long-term channel SNR adaptation would help to implement adaptive modulation. Figure 4.13 shows the simulation results of improved long term SNR estimation with FFT and perfect channel assumption in the presence of BER target 1%. Table 4.5 summarizes the parameters used for the simulation results of Figures 4.13.

4.7.2 Effect of Doppler frequency

As discussed previously, Doppler frequency has a strong impact on the performance of shorter term SNR estimation and adaptation. Doppler frequency is directly related to how fast the vehicle is moving with respect to the transmitter. We would thus like to examine the explicit impact of Doppler frequency on the performance of long term estimation and adaptation. Figures 4.14 (a) and (b) show simulated results for various Doppler frequencies and Table 4.6 summarizes the parameters used for the simulation of Figures 4.14.

Table 4.6 Specifications used for the simulation results of Figures 4.14

Pilot symbol spacing	64
Doppler frequency	10Hz
Frame rate	500Hz
Frame length	64 symbols
Symbol rate	32kHz
Frame duration	2ms

BER = 1%, Perfect channel assumed, Improved Long Term SNR estimation

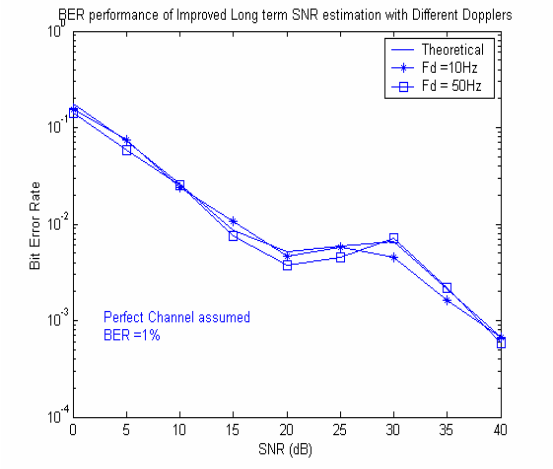

Figure 4.14 (a) BER performance of adaptive modulation with different Doppler frequency

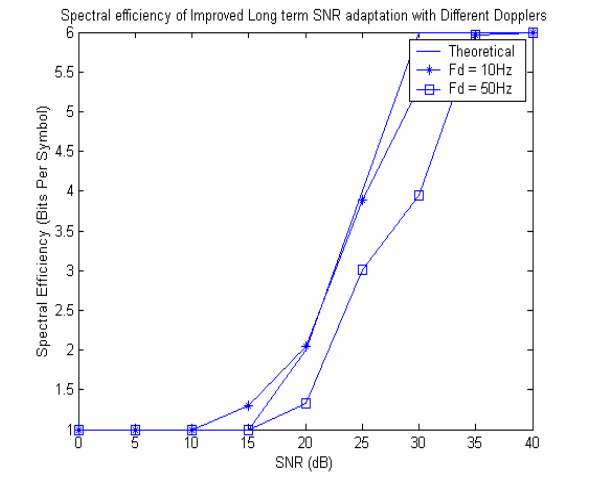

Figure 4.14 (b) Spectral efficiency of adaptive modulation with different Doppler frequency

It should be noted that the short term adaptive modulation technique doesn't perform well in case of the fast fading channel since the SNR estimation will no longer remain constant over the frame in a fast fading channel. However, with long term estimation we

do not see this same magnitude of degradation. Thus, overall performance of improved Long term SNR estimation is very promising at higher Dopplers or in fast fading channel.

4.7.3 Effect of equalization techniques

Finally, we would like to investigate the effect of channel equalization on the adaptive modulation using the improved long term SNR estimation. Figure 4.15 shows the performance of adaptive modulation at a target BER of 1% in the presence of FFT interpolation at a Doppler rate of 10Hz. We notice that the use of FFT interpolation does not impact the performance of long term estimation nearly as much as short term estimation. This is because in long term SNR estimation we are averaging the signal energy over a large period of time and is thus insensitive to delay. Therefore, we avoid the edge effects associated with FFT interpolation by using the middle frame for both demodulation and SNR estimation.

BER = 1%, FFT interpolation, Improved Long Term adaptation

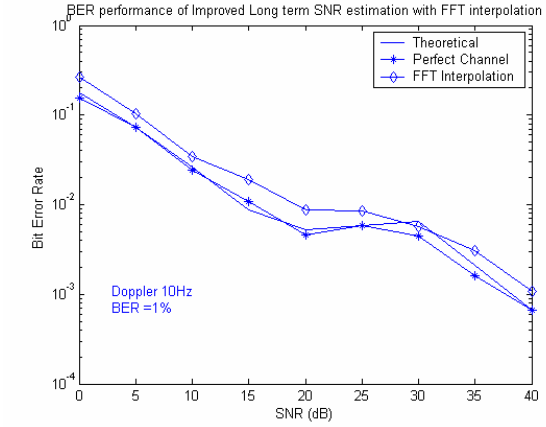

Figure 4.15 (a) BER curve for the adaptive modulation with Doppler =10Hz

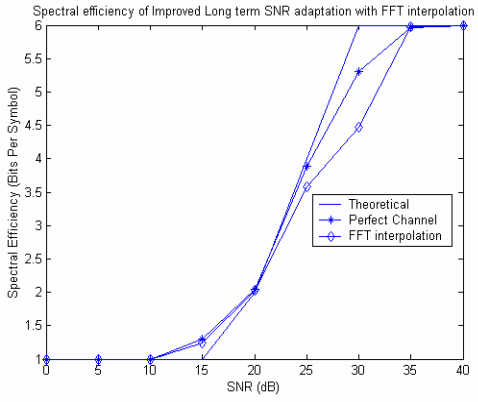

Figure 4.15 (b) Spectral efficiency of the adaptive modulation with Doppler = 10Hz

4.8 Chapter summary

In this chapter we examined the effect of SNR estimation on the performance of adaptive modulation. Specifically we showed that in slow fading channels, SNR estimation has virtually no effect on performance or spectral efficiency. However, at high Doppler spreads, SNR estimation has a profound impact on both performance and spectral efficiency. We further showed that using an improved SNR estimate that accounts for channel variation allows us to reduce the degradation in spectral efficiency, but we cannot eliminate the BER performance degradation. This is because the degradation is not due to the SNR estimation but is simply due to the fact that adaptation is slower than the channel variation. Further, we found that when using FFT interpolation the degradation in spectral efficiency cannot be avoided due to the edge effects. The edge effects could be avoided if a delay in SNR estimation could be tolerated. However, this is not possible with short term estimation and adaptation.

BER 1%, Doppler frequency = 50Hz, Improved Long Term SNR estimation, FFT Channel interpolation

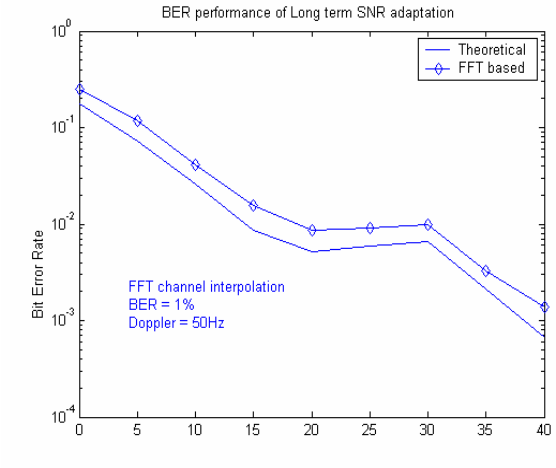

Figure 4.16 (a) BER performance of Improved Long Term Adaptive Modulation

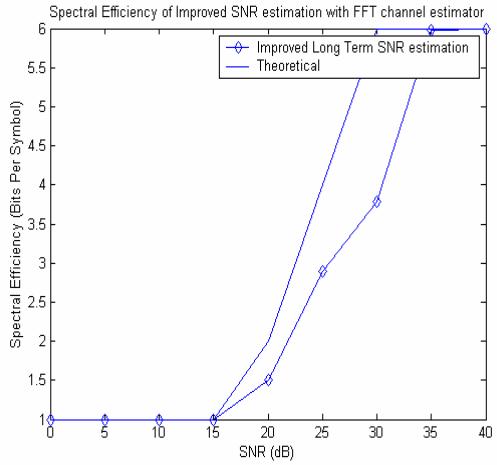

Figure 4.16 (b) Spectral efficiency of Improved Long Term Adaptive Modulation

BER 1%, Doppler frequency = 50Hz, Improved Short Term SNR estimation, FFT Channel interpolation

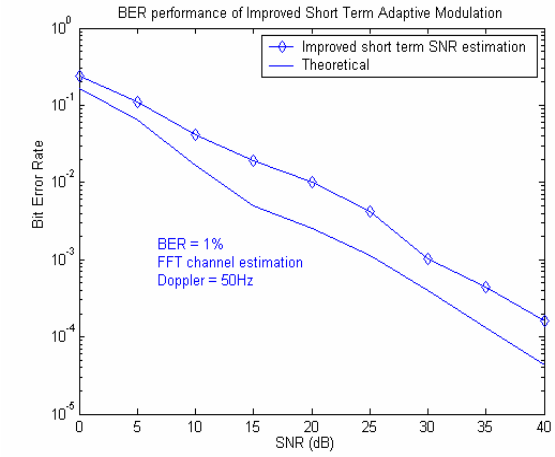

Figure 4.16 (c) BER performance of Improved Short Term Adaptive Modulation

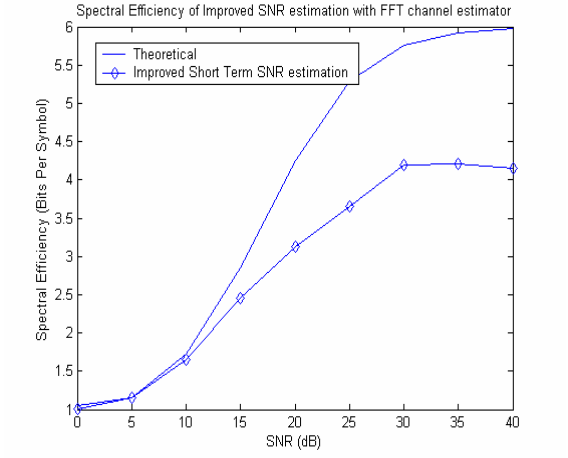

Figure 4.16 (d) Spectral efficiency of Improved Short Term Adaptive Modulation

This led us to consider long term estimation which attempts to estimate the long term or average SNR over some window. This technique is insensitive to delay and thus we could use the improved SNR estimation technique in high Dopplers even when using FFT interpolation. Thus, in Figure 4.16, long term estimation is shown to suffer less degradation in spectral efficiency and performance due to Doppler than short term estimation. However, the drawback to long term estimation is that it provides a slightly worse trade-off between energy efficiency and bandwidth efficiency than short term estimation. This is because in short term estimation we attempt to always use the optimal modulation scheme. In long term estimation we are using the modulation scheme that is optimal based on the *average* SNR. However, long term estimation is still better than static modulation.

Chapter 5 CONCLUSIONS AND FUTURE WORK

5.1 Conclusions

In this thesis work, we have investigated the factors which influence the performance of adaptive modulation. Of primary focus was the impact of channel estimation and channel quality (SNR) estimation. The performance was measured in terms of both spectral efficiency and bit error rate. Various channel estimators were investigated in Chapter 2 for use with QAM modulation in flat fading channels. We showed that the FFT based channel estimators provide more accurate interpolation as compared to Gaussian and Wiener interpolation. Adaptive modulation was introduced in Chapter 3. The basic idea of adaptive modulation is to improve combined spectral efficiency and energy efficiency by using BPSK and QPSK when the channel is very poor and QAM when the channel is good. Simulation results were provided for adaptive modulation in the presence of different channel estimators, feedback delays, and Doppler frequencies. We investigated the impact of these factors on BER performance and spectral efficiency. In Chapter 4 we provided an analysis of adaptive modulation with SNR estimation. We investigated a modified version of the maximum likelihood estimator as well as an improved short-term estimator for fast fading channels. We concluded Chapter 4 with an investigation of long term SNR estimation. With long term estimation, we adapt modulation only to the long term or average SNR. We provided a comparison of the improved short and long term SNR adaptation techniques. We showed that long term SNR estimation has an advantage in fast fading since it is tolerant of feedback delay.

5.2 Future work

Our work provides insight into some of the practical issues associated with adaptive modulation. We summarize here a few potential future directions for this work.

1) We assumed constant transmit power in use of adaptive modulation. It would be interesting to study adaptive modulation that also used variable transmit power

level. As shown earlier, from an information theory point of view, constant power adaptation provides nearly equivalent performance as variable power. However, it would be of interest to examine the difference with specific modulation and coding schemes.

2) Most data communication systems use coding technologies to reduce bit error. Convolutional coding is typically used for this purpose. Therefore, studying adaptive modulation with adaptive coding is another possible area of investigation [18].
3) All of the simulations in this work have assumed flat Rayleigh fading. The effect of frequency selective fading on adaptive modulation would also be of interest.
4) Analyzing the impact of feedback error in the adaptive modulation would be of interest.
5) The implementation of adaptive modulation on a software radio platform.
6) Improving the performance of adaptive modulation using channel prediction.

These are but a few possible extensions to the current work that would make interesting investigations.

BIBLIOGRAPHY

[1] J. M. Torrance and L. Hanzo, "Upper bound performance of adaptive modulation in a slow Rayleigh fading channel," *IEEE Electronics letters*, Volume 32, Page(s): 718-19, April 1996.

[2] L. Hanzo, W. Webb and T. Keller, Single- and Multi-carrier Quadrature Amplitude Modulation, Principles and Applications for Personal Communications, WLANs and Broadcasting,, IEEE press, New York, 2000.

[3] J. K. Cavers, "An analysis pilot symbol assisted modulation for Rayleigh fading channels," *Transaction IEEE Vehicular Technology*, Volume: VT-40, No. 4, Page(s): 686-93, November 1991.

[4] E. Okamoto, L. Huan-Bang and T. Ikegami, "Rayleigh fading compensation for QAM by using FFT", *Proceedings of the Seventh IEEE International Symposium on Personal, Indoor and Mobile Radio Communications, PIMRC'96,* , Volume: 3, Page(s): 1079 - 1082, 1996.

[5] C. Bang and M. H. Lee, "An analysis of pilot symbol assisted 16 QAM in the Rayleigh fading channel", *IEEE Transactions on Consumer Electronics*, Volume: 41, Number 4, Page(s) : 1138-1141, November 1995.

[6] S. Sampei and T. Sunaga, "Rayleigh fading compensation for QAM in land mobile radio communications," *Transaction IEEE Vehicular Technology*, Volume: 42, Number 2, Page(s): 137-47, May 1993.

[7] S. Sampei, A Publications of Digital wireless technologies to Global wireless applications. Englewood Cliffs, NJ: Prentice Hall, 1977.

[8] T. S. Rappaport, Wireless communications: Principles and Practice, Prentice Hall Inc., New Jersey, 1996.

[9] W.C. Jakes (ed), Microwave Mobile Communications, IEEE press, New York, 1974.

[10] E. Okamoto, L. Huan-Bang and T. Ikegami,"A Pilot Symbol Assisted Compensation Scheme of Fading and Frequency Offset for 16QAM", *IEEE International Conference*

on Universal Personal Communications, ICUPC, Volume: 2 , Page(s): 921 –924, 1998.

[11] J. Cavers, "Pilot Symbol assisted modulation in fading and delay spread," in *IEEE Transactions on Communications, Vehicular Technology Conference*, (Secaucus, NJ, USA), Page(s). 13-16, IEEE, May 18-20,1993.

[12] T. Xiaoyi, M. S. Alouini and A. Goldsmith, **"** Effect of channel estimation error on M-QAM BER performance in Rayleigh fading ", *Vehicular Technology Conference, 1999 IEEE 49th* , Volume: 2 , Page(s): 1111 -1115, 1999.

[13] A.Goldsmith and S.G. Chua,"Variable – Rate Variable –Power MQAM for fading channels,". *IEEE Transactions on Communications*, Volume 45, Number 10, October1997.

[14] K. Balachandran, R. K. Srinivas and N. Sanjiv,"Channel Quality Estimation and Rate Adaptation for Cellular Mobile Radio,". *IEEE Journal on selected areas in communications*, Volume 17, Number 7, July1999.

[15] J. Proakis, Digital Communications, McGraw Hill, 3rd., 1995.

[16] R.M. Gagliardi and C.M. Thomas, "PCM data reliability monitoring through estimation of the signal-to-noise ratio," *IEEE Transactions on Communications,* Volume COM-16, Page(s). 479-486, June 1968.

[17] M. Abramowitz and I.A. Stegun, Handbook of Mathematical Functions, Dover Publications, New York, 1970.

[18] M.D. Austin and G.L. Stuber, "In-Service Signal Quality Estimation for TDMA Cellular Systems", *Proceedings of the Sixth International Symposium on PIMRC.*, Volume: 2 , Page(s): 836 –840, 1995.

VITA

Payal Jain was born on May 20, 1976, in Michigan, USA. She received her B.Tech. degree in electrical and computer engineering from J.M.I., a central government university at New Delhi, India in 1999. She worked as a Project Trainee at Electrotech, Roorkee, India. She enrolled in the Masters program in electrical engineering at Virginia Tech in 2000. From Fall 2000 to Fall 2001, Payal served the department of electrical and computer engineering at Virginia Tech as a graduate teaching assistant, teaching Electronic Networks laboratory. She then joined Mobile and Portable Radio Research Group under the guidance of Dr. R. M. Buehrer in December 2001. Presently, she is working as a DSP Engineer at Digital Receiver Technology, Maryland.